IEEE Journal of Microwaves

Received 24 October 2023; accepted 2 December 2023. Date of publication 29 December 2023; date of current version 8 January 2024.

Digital Object Identifier 10.1109/JMW.2023.3341228

Electromagnetic and Electronic Aerospace Conformal Load-Bearing Smart Skins: A Review

GRZEGORZ BEZIUK[1] (Member, IEEE), ANDREW KRAJEWSKI[2] (Member, IEEE), THOMAS C. BAUM[1] (Member, IEEE), KELVIN J. NICHOLSON[1] (Senior Member, IEEE), AND KAMRAN GHORBANI[2] (Senior Member, IEEE)

(Invited Paper)

[1]Defence Science and Technology Group, A V Division, Melbourne, VIC 3207, Australia
[2]School of Engineering, RMIT University, Melbourne, VIC 3000, Australia

CORRESPONDING AUTHOR: Kamran Ghorbani (e-mail: kamran.ghorbani@rmit.edu.au).

This work was supported by the Defence Science Technology Group, NGTF Australia.

ABSTRACT Multifunctional composite structures (MFCS) have become an increasingly important field of research with the large-scale adoption of composite materials in many industrial sectors such as aerospace, automotive, sport and recreation equipment (bikes, scooters, etc.) and maritime. It is a diverse field which includes scientific areas in electromagnetics, electronics, material sciences, structures and structural augmentation, sensors, and thermal management. The paper investigates Conformal Load-bearing Smart Skins (CLSS) as a part of multifunctional composite structures specifically related to aerospace applications and focuses on the seamless incorporation and synergistic coexistence between electronic devices and composite materials. Current trends in materials and manufacturing processes, as well as measurement techniques used to validate both the electromagnetic and structural responses have been explored and discussed. Furthermore, it identifies some of the challenges and complexities associated with CLSS and explores future areas of research which still need to be addressed.

INDEX TERMS CLAS, CLSS, load-bearing microwave structure, load-bearing smart skins, multifunctional microwave structure.

I. INTRODUCTION

Research in the area of CLSS has increased recently and can be judged by the number of publications per year released within the last three decades. Based on the 179 publications used as references in this review paper, the research in CLSS technology and applications has increasing since 2005 - 2006 (Fig. 1). It coincides with growing interest in unmanned aerial vehicles (UAV) and their use in both civilian and military applications. CLSS are formed using multidisciplinary concepts which typically focus on the synergistic design of composite structures that combine electrical/electronic functions, however, other disciplinary areas have also been explored.

The field of CLSS finds major contributors in countries with considerable knowledge and manufacture/processing of composite materials (Fig. 2.). The three main contributors by publication in this field include the USA, Australia and China with many other significant contributions from Europe, U.K., Middle East and Asia.

With rapid advancement and up-take of UAVs, there has been a drive to make them smaller, more functional, more versatile and cheaper. This has resulted in the need for higher levels of integration and miniaturization of electronics in these systems. CLSS provide a possible avenue for realizing some of these goals by allowing designers to more efficient utilize the volumetric constraints posed by these small platforms.

The concept of Smart Skins for aerospace applications was first presented in 1990 by Thomas [1], as shown in Fig. 3, and it was inspired by US Air Force's "Project Forecast II" [2]. Thomas discussed four areas of possible system integration: (i) radio-frequency (RF) antennas and systems, (ii)

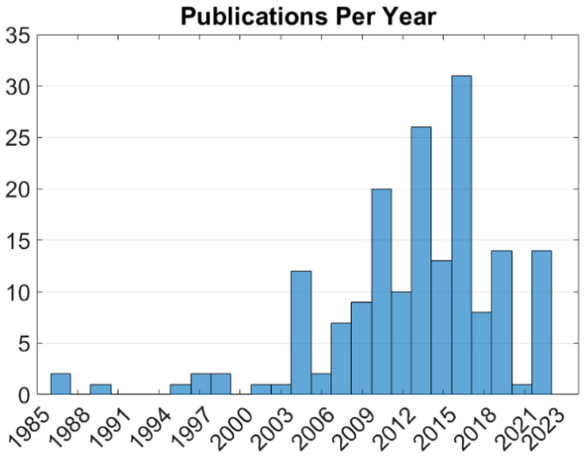

FIGURE 1. Publications per year for CLSS technologies.

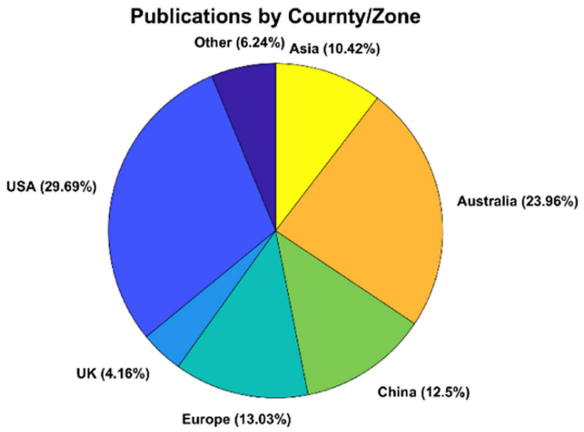

FIGURE 2. Number of publications per country.

structural health monitoring sensors and systems, (iii) thermal management structures and lastly (iv) distributed avionic architectures.

Broadly, smart skin structures are a technology concept that allow the integration of advanced sensors, actuators, and micro-processors into the skin of flying vehicles with the aim of improving their overall performance. The objective is to self-diagnose faults, self-adapt to external or internal conditions, self-learning about its structural conditions, and self-repair when correction is needed. Smart Skins for structural health monitoring (SHM) in section (ii) of Thomas's paper received extensive attention in the preceding years and is still an active field of research.

The goal of this paper is to review past and recent activities in the development of CLSS relating to the other field highlighted in Thomas's paper. Specifically, it will focus on the field of research relating to: radio-frequency (RF) antennas and systems, thermal management structures and distributed avionic architectures. This review is broken up into four main topic areas which will explore the most up-to-date and state-of-the-art progress in this field.

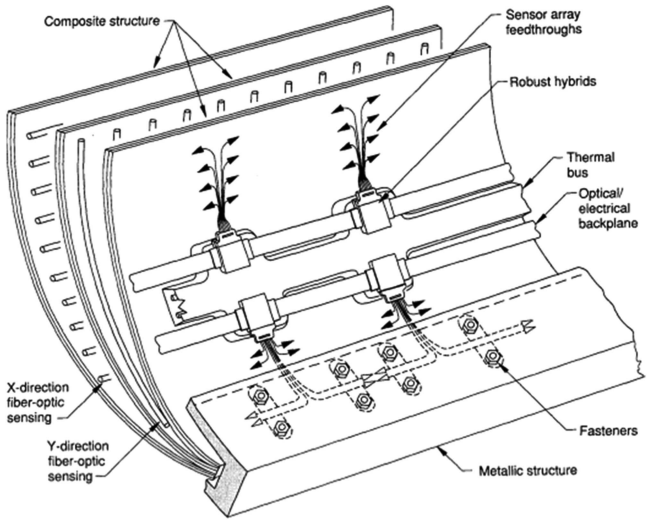

FIGURE 3. Thomas's concept of the smart skin [1].

Section II of this work will discuss the properties of the materials used for CLSS manufacturing and their implementations in load bearing skins. Material selection and formulations are a critical part to realizing the functionalities of CLSS. The materials used by various authors have been reviewed and categorized with regard to the end functions and properties. This includes a review of load bearing materials used in different proposed concepts, as well as functional materials such as dielectrics and conductors. This section will also cover a large variety of different fabrication methodologies involved in manufacturing CLSS structures.

Section III will describe the testing and validation methods according to the designed functionalities of CLSS structures (i.e., RF/communication, navigation, sensing, structural, flow, pressure, etc.). Hybrid testing of CLSS structures and validation of their performance has been reviewed to confirm the bounds of the proposed concepts. Testing and validation of disciplinary fields are typically well established, however the notion of CLSS required unique testing and validation processes specific to their desired functionalities. The challenges associated with this have been explored and possible future challenges are also outlined in this chapter.

Section IV of this work provides a review of existing application of CLSS technology. CLSS is widely proposed as a way of achieving more efficient volumetric utilization and hence is proposed to achieve better Size, Weight and Power (SWaP) in various applications. Section IV is split into four sub-sections focusing on antennas, electronics and RF systems, sensors, and thermal management.

Sub-section A (antennas) explores the integration and performance aspects of different high performance antenna topologies for use in CLSS applications. It also includes a review of the integration and manufacturing processes used to realize these structures.

Sub-section B (electronics and RF systems) explores concepts relating to the integration of dedicated electronic circuitry and other electronic RF systems into CLSS applications. Various types of electronic and RF systems applications within the CLSS hybrids are discussed.

Sub-section C (sensors) explores a variety of sensor concepts that have been integrated into CLSS hybrid structures. It touches on unique applications where the proposed sensor concepts differ from traditional SHM technologies or provides a SHM solution using RF systems.

This review also dwells on the application of CLSS sensing systems for monitoring and controlling different structural parameters.

Finally, Sub-section D (thermal management) explores the thermal management of CLSS structures and its impact on their performance. This section is conspicuous in any review of technology especially when it is linked to the area of high-performance avionics/electronics which can generate heat. This work presents examples of thermal management used to improve the performance of these complex CLSS structures.

Section V will identify and provide the key challenges in developing more advanced CLSS structures technologies. It will also identify some of the missing gaps in CLSS research. Future prospects of CLSS multifunctional technologies specifically related to the aerospace industry will also be considered.

Finally, Section VI will provide short conclusions that summaries this work.

In reference to the types of CLSS structures being reviewed within the sections outlined above there are six main categories that the technologies can be described. There are: Conformal Load-bearing Antenna Array Structure (CLAAS), Conformal Load-bearing Antenna Structure (CLAS), Conformal Sensors (CS), Conformal Load-bearing Electrical and Electronics (CLEE), Conformal load-bearing power generation (CLPG), and Conformal Load-bearing Thermal Management (CLTM). There are also two analysis categories covering material evaluation and mechanical evaluation.

II. MATERIALS AND MANUFACTURING

This section of the review identifies and categorizes the large variety of materials used for realizing CLSS. It explores materials such as fiber reinforce polymers, resins, conductor and dielectrics which are formulated and structured to realize CLSS.

A. CLSS MATERIALS

Material selection forms a critical part in the design process of load-bearing smart skin structures. Accelerated advancements in materials research over recent years provided desirable electrical and mechanical characteristics for both conductors and insulators. Many of these new materials typically fall under the banner of micro and nanomaterials. Broadly, the objective of the CLSS materials used in aerospace applications are to provide excellent conductivity, mechanical and thermal properties. A mixture of materials used in CLSS depends on the function the structure must perform. For example, diverse materials are used in skins that embed elements for communication (RF) compared to those that embed elements for structural monitoring or other types of sensing. Ideally, the materials should be flexible and be able to form specific shapes before being bonded together. Strong adhesion between them is vital to their mechanical and electrical performance. The strength of a bonded structure should not differ from the rest of the skin on an aircraft or UAV.

Carbon Nanotubes/Fibers Related Materials: There are multiple examples of using high density vertically aligned carbon nanotubes (CNT) [39] printed on a polymer substrate to fabricate load-bearing conformal microstrip antennas. For example, the antenna in [39] operated at a center frequency of 2.2 GHz and achieved 5 dBi of gain.

Unidirectional Carbon Fiber tows have been used to manufacture flexible Micro-Air-Vehicles (MAV) [142]. The electronic components use micro hot-film sensors to control and improve the MAV's performance.

Dissimilar composite materials were fused to create load bearing RF antennas in [152], [152], [153], [154]. The authors in [154] successfully tested joints between Carbon/Epoxy and Glass/Epoxy in multi-ply mechanical configurations. They assessed and compared the strength of joints between the following composite fiber structures: Carbon-carbon, glass-glass, carbon-glass. They concluded that the strength of the hybrid composite joint was approximately 50% of the strength of an un-notched unidirectional glass fiber composite.

Liquid Metal Related Materials: Embedded micro vascular channels filled with liquid metal have been used to create arms of a reconfigurable meandering dipole antenna [40], [41], [42]. The reconfiguration of the antenna was achieved by controlling the amount of the eutectic metal alloy of Gallium-Indium (EGaIn) injected into micro-vascular channels. This in turn changed the overall length of the dipole arms and hence provided a means to tune its frequency response.

E-textiles/Conductive Textiles Related Materials: Conductive textiles (e-textiles) are another type of flexible material that has been used in manufacturing of smart skin structures. Electrodeposition of metals on Kevlar fibers or NOMEX have been used to generate conductive yarn which in turn may be woven, knitted or embroidered into glass/carbon fiber sheets creating the desired RF response [49]. Electrical conductivity of a textile may also be achieved by dying with conductive nanomaterials. The successful manufacture of a planar conformal lightweight patch antenna was demonstrated in [43]. This e-textile was fabricated by dyeing a fabric with single-wall carbon nanotubes (SWNT). Silver was sputtered on the dyed SWNT fabric to improve its conductivity. Another approach to e-textiles is to weave conductive yarns into fabrics. A silver coated nylon / polyester yarn was used in [44], [45], [46] to manufacture microstrip patch antennas. The radiating path, feeding line and ground plane were all woven into glass fabrics using solid copper yarns. Authors of works [47], [48], [49], [50], [51], [52] demonstrated use of conductive yarns to realize e-fiber antennas. The conductive coated polymeric

silver-coated Zylon fibers (e-fibers) were used to fabricate conducting elements of a patch antenna in [47] and [48]. The e-fibers were embroidered on the top and bottom layers of a polydimethylsiloxane polymer composite creating a conformal radiator for UAV applications. This antenna operated at a center frequency of 2.2 GHz with a gain of 5.7 dBi.

In [49] the authors presented the development of a load bearing electrically small Egyptian Axe Dipole (EAD) antenna embedded into an aerospace composite structure. The antenna used a structural glass (S-Glass) fiber impregnated with Hexply 914E epoxy resin. The UHF antenna elements were sewn using a computer-controlled embroidery machine. The conductive yarn used in this example was a silver coated Shieldex 110/34f thread. To improve the EAD antenna performance, the device was redesigned and fabricated again using different materials. The authors specifically investigated materials with lower-loss dielectrics and high conducting materials [50], [51]. The new design incorporated a foam sandwiched structure where the EAD was sewn using a conducting Aracon XS0200E-025 thread (a Kevlar thread with a silver metallic coating). The composite skins which include the EAD elements, comprised of high purity Quartz (Astro-Quartz) fabric and a low loss cyanate ester resin. The change in materials resulted in a 5.9 dBi increase in the EAD gain. The same materials (conductive Kevlar fiber Aracon XS0200E-025; prepreg Hexply 914E and a cyanate ester resin structural glass composite) were used to fabricate several patch antennas [52]. This work investigated the effect of thread orientation on the performance of these patch antennas highlighting the anisotropic nature of the conducting materials.

Non-Woven Materials: Non-woven materials have also been utilized to fabricate CLSS. Veil materials consist of short, chopped fibers which are held together with a weak binder. These materials provide a more consistent and uniform conductivity compared to e-textile approaches. Typically, the fibers consist of carbon, carbon-nickel, carbon-nickel-copper, or silver coated polymer fibers. These materials are attractive as they can be laser cut, transferred, and will easily consolidate in traditional composite structures due to their high porosity. Carbon-nickel-copper veil was used to fabricate an EAD antenna in [51], [53]. The antenna measurements indicated that the conductor's RF performance is better than conductive threads, however it has a slightly lower conductivity compared to solid copper foil due to its porosity and effective surface roughness.

Conductive Paint and Inks Related Materials: There have been a many examples where high-quality conductive paints or inks used in the process of fabricating CLSS structures. For example, an integrated waveguide and horn antenna [54] was 3D printed using ABS plastic and subsequently covered with silver conductive paint. Another example of using nanoparticle ink is presented in [55] where the authors presented a conformal load-bearing antenna structure (CLAS) for UAV applications. They utilized the aerosol jet printing in an nScrypt 3Dx-700 to accurately deposit commercially available concentrated copper nanoparticle ink directly onto a cured epoxy S-Glass fiber-reinforced pre-preg which was then cured. A copper-coated carbon veil was used to print ∼2.4 GHz patch antenna in order to create conceptual CLAS as a part of the UAV's wing skin. The structure was later assessed with regard to the impact of mechanical loading and antenna performance [173].

Load-bearing antenna structures with embedded flexible electronics are presented by Chaney [150]. They use a FleX^{TM} Silicon-on-Polymer^{TM} process to fuse standard Si (silicone) wafers into flexible structure. The materials used are silicon wafers, flexible polymer sheets as a carrier and metallic paste as a conductive element.

Development of UAVs has progressed research into power harvesting and generation. It achieved this by embedding solar elements in the wings of an aircraft or UAV. The aim was to extend the endurance of the UAV. The researchers in [140], [141] simulated electrical performance of various combinations of mono/polycrystals based photovoltaics and polymer based photoelements. The panels were fused into the fixed-wing composite structure of the UAV. A GaAs thin film photovoltaic (Sunpower 60) was used during a successful test, increasing battery charge by 10% which extended flight time of the UAV by 2 minutes [141].

Mirotznik et al. [143] analyzed the suitability of structural composites with embedded microstrip transmission lines (fabricated using etched copper shim or screen-printed silver ink) for RF application. The authors used BTCy-1 6781 (S-Glass / Cyanate Esters GFRP) with $\varepsilon_r = 4.2$ and $\tan(\delta)$ 0.004 as the substrate. Tables 1 and 2 summarize the non-conductive and conductive materials used to manufacture multifunctional composite structures.

B. MANUFACTURING TECHNIQUES

Development of a structurally integrated conformal load-bearing multifunction smart skins require a manufacturing process that involves bonding a variety of materials. The aim is to provide rigidity high enough so as not to degrade the structural integrity of an aircraft's skin.

A typical smart skin panel assembly is shown in Fig. 4. The manufacturing process involves cutting pre-preg sheets into the desired shapes and laminating them over a mold before curing under vacuum in an autoclave. This laminating step allows for the easy addition of a radiating element in the stack-up.

An absorber assembly may be manufactured separately and bonded to the inner surface of the CLASS panel [4], [5], [6], [7]. The panel is then bonded to the wing becoming an integral part of the aircraft's structure.

A similar manufacturing process was presented in [132]. The manufacturing process consisted of two steps: First fabrication of main load-bearing composite structure and RF transparent housing. Manufacturing steps included: (i) manufacture of the mold tool, (ii) pre-preg cutting to the desired shape by mechanical tools, (iii) laying up the pre-preg layers in the mold. (iv) autoclave curing, (v) non-destructive inspection, (vi) trimming and machining the structure. Step two dealt

TABLE 1. Summary of Non-Conductive Materials

Materials	Dielectric	Tanδ	Application	Freq.	Ref No.
ABS	-	-	CLAS	7.5 - 18GHz	[54]
AF-126 Adhesive	-	-	CLAS	-	[125]
Air	1.0059	-	CLAAS, CLAS	0.163 - 10GHz	[23], [37], [38], [69]-[78], [83], [84], [130], [159], [160]
Balsa Wood	1.2	-	CLAAS	2.45GHz	[21], [22]
Bismaleimide Triazine (BT)	-	-	CLEE, CLPG	-	[151]
BMI	-	-	CLAS	-	[3]
Cyanate Ester / GFRP (S-Glass)	3.26 - 4.23	0.003-0.005	CLAAS, CLEE	0.01-12GHz	[52], [131], [143], [147], [174]
Cyanate Ester Resin	2.7	-	CLEE	2.4GHz	[174]
DP460 Epoxy	-	-	CLEE, CLPG		[151]
ECCOSTO CK® HiK/polyetheretherketone(PEEK)	3.3	-	CLAS	1.159 - 1.949GHz	[35]
E-Glass Fiber	6	0.001	CLAS	-	[126]
Emerson & Cuming's HiK	12	0.0007	CLEE	2.4GHz	[174]
Epoxy Bonding Film	3-3.15	0.0221-0.025	CLAAS	2.5 - 12.5GHz	[12], [13]
Epoxy Resin	4.5	0.02	CLAS		[126]
Ferrite Absorber			CLAS	0.2 -1.2GHz	[29]
Ferro A6-S	5.9	0.002	CLAAS	29 - 31GHz	[137]
FLeX-IC	-	-	CLEE		[150]
FM300M	-	-	CLTMl		[136]
Foam	-	-	CLAAS	VHF - 3.9GHz	[158], [162]
Foamclad R/F 100	1.25	0.0035	CLAS	1.41 - 4 GHz	[36]
FR4	4.4-4.8	0.017-0.02	CLAAS, CLAS, CS, CLEE, Mechanical Evaluation	0.3 - 10GHz	[17], [18], [20]-[22], [25], [26], [32], [34], [40], [42], [96]-[101], [118]-[122], [129], [172]
GFRP (E-Glass)	4-5.25	0.01-0.036	CLASS, CLAS, CLEE, CLPG	0.4 - 31GHz	[4]-[13], [23], [24], [44]-[46], [81], [82], [115], [116], [127], [128], [137], [151], [162], [170], [173], [179]
GFRP (S-Glass)	3.375-4.375	0.0141-0.025	CLAAS, CLAS, CS, CLEE, Mechanical Evaluation	DC - 10GHz	[3], [33], [49], [50], [52], [53], [55], [79], [106], [144]-[146], [148], [149], [152]-[158], [163], [165], [166], [168]
Hexafettire-Glass	7.44 (μ_r = 2.02)	0.005 (Tanδμ = 0.08)	CLAS	2.48GHz	[34]
High Density Polyethylene (HDPE)	1.15	0.000227	CLAS	2.44GHz	[164]
Kapton	-	-	CLAS	2.08GHz	[27]
KRFP (Kevlar)	4	-	CLAS	2.08GHz	[27]
LWF-2	3.14	0.0221	CLAS	1.25 - 1.6GHz	[163]
MCT-PDMS Composite	3.8	0.015	CLAS	2.2GHz	[39]
NOMEX	1.1-1.12	0	CLAAS, CLAS	0.2 - 12.75GHz	[4]-[13], [15], [29], [115], [116], [125]
PDMS	3	0.02	CLAS, Mechanical Evaluation	DC - 6GHz	[48], [124]
PDMS-RET Composite	3.8	15	CLAS	2.2GHz	[47]
PDMS-Strontium Titanate (ST)Composite	3 to 13	0.01	CLAS	2 and 2.4GHz	[43]
Polyamide	2.6 - 3.5	0.0013 - 0.0026	CLAS, CS, CLEE, CLTM	2 - 40Ghz	[90]-[101], [115], [116], [135], [142], [167]
Polymethacrylimide (PMI) Foam	1.1-1.3	0.005-0.012	CLAAS, CLAS	2 - 40Ghz	[137] , [167]
Polyurethane Foam (FR-6718)	-	-	CLTM	-	[133]
Pyralux FR8510R	3.5	0.02	Mechanical Evaluation	-	[123]
QFRP	3.2-3.66	0.002-0.0061	CLASS/CLAS	0.015 - 40GHz	[4]-[7], [40]-[42], [50], [52], [53], [132], [167]
Rogers RO 4003	3.38-3.55	0.002	CLAAS, CLAS	1.5 - 7.5GHz	[14], [15], [125]
Rogers RO 4350B	3.66	0.037	CLAAS	2.45 - 5.8GHz	[16], [115], [116]
Rohacell 100WF	1.14	0.0022	CLAS	1.25GHz, 1.6GHz	[163]
Rohacell HF	1.0449-1.07	0.0002-0.0003	CLAS	0.3 - 6.5GHz	[27], [50], [51], [53], [71]
Rogers RT/Duroid 5880	2.2	0.0009	CLAAS, CLAS	0.3 - 12.75Hz	[9]-[13], [71], [76]-[78], [85], [86]
Styrofoam			CLAS	0.48GHz	[28]
SU-8	3.25	0.0155	CLAS	2.44GHz	[164]
Taconic TLY5-0600-C1/C1	2.2	0.0009	CLAS	5.6GHz	[19]
UD-CFRP	29.7 to 31.4	0.24	CFRP Material Evaluation	-	[58]

CLAAS – Conformal Load-bearing Antenna Array Structure
CLAS - Conformal Load-bearing Antenna Structure
CS – Conformal Sensors
CLEE – Conformal Load-bearing Electrical and Electronics
CLPG – Conformal Load-bearing Power Generation
CLTM – Conformal Load-bearing Thermal Management

TABLE 2. Summary of Conductive Materials

Material	Conductivity	Application	Freq.	Ref No.
Aluminum	3.56e7 S/m	CLAAS, CLAS, Mechanical Evaluation	0.48 - 31 GHz	[23], [28], [32], [74], [77], [121], [125], [137], [139], [164]
Aluminum Honeycomb	-	Thermal	-	[136]
CFRP	15 - 51e3 S/m	CLAAS, CLAS, CS, CLEE, CLPG, CLTM, Mechanical Evaluation	0.04 - 12GHz	[3], [29], [38], [52], [56]-[59], [62]-[79], [81]-[87], [117]-[119], [121], [123], [130]-[133], [136], [138], [151]-[156], [158]-[166], [170]
CFRP-MWCNT Composite	150 to 4000 S/m	CLAS	1 - 10GHz	[80]
CNT	1 Ω/□	CLAS, CS	2.2GHz	[39], [106]
Copper	5.8e7 S/m	CLASS, CLAS, CS, CLEE, CLTM, Mechanical Evaluation	DC - 31GHz	[3]-[22],[24]-[26], [29]-[31], [33]-[38], [40], [49], [51]-[53], [55], [77], [81], [82], [84], [86], [88], [89], [90]-[101], [115]-[122], [125], [127]-[129], [135], [142], [144]-[149], [157], [158], [162]-[166], [169], [171], [172], [174]
Copper Ink	-	CLEE/CLPG	-	[151]
Copper Plated Silver Ink	2e6 S/m	CLAS	10GHz	[55]
Copper Yarn	0.2 to 0.36 Ω/m	CLAAS, CLAS	1.5GHz	[44]-[46], [126]
Galinstan	3.57e6 S/m	CLAS	0.766 - 3.165GHz	[40] - [42]
MWCNT	-	Mechanical Evaluation	-	[124]
Ni-Cu-Ni-Ag plated Kevlar yarn	-	CLAS	1-5 GHz	[168]
Resistive Sheet	-	CLAS	2-40 Ghz	[167]
Silver Epoxy	-	Mechanical Evaluation	-	[123]
Silver Ink	3.3e5 - 1e6 S/m	CLAS, CLEE	0.01 - 8GHz	[27], [143], [144], [148], [150]
Silver Paint		CLAS, CS	7.5 - 18GHz	[54], [106]
Silver Paste		Mechanical Evaluation	0.18 - 0.2GHz	[117]
Silver Yarn	0.02 - 0.45Ω/□ and 0.8-65 Ω/m	CLAS	DC - 6GHz	[47]-[53], [79], [145], [146], [149]
SWCNT	1-2 ohms	CLAS	2 - 2.4GHz	[43]
Veil - Carbon	5333 S/m	CLAS	2.4GHz	[173]
Veil - CNC (C-Ni-Cu)	1.5e6-2e6 S/m	CLAS, CLEE, Material Evaluation	0.01 - 8GHz	[51], [53], [60], [61], [66], [144], [147]-[149], [179]

with the radiating element and consisted of: (i) cutting pre-pregs using a mechanical cutter, (ii) laying up the pre-pregs, (iii) vacuum bagging (iv), and curing in the autoclave.

The manufacturing processes described above are widely used in smart skins fabrications. The aim is to create a rigid structure where active or passive components are sandwiched between the top and bottom layers of a skin. The materials may differ from each other depending on the desired function.

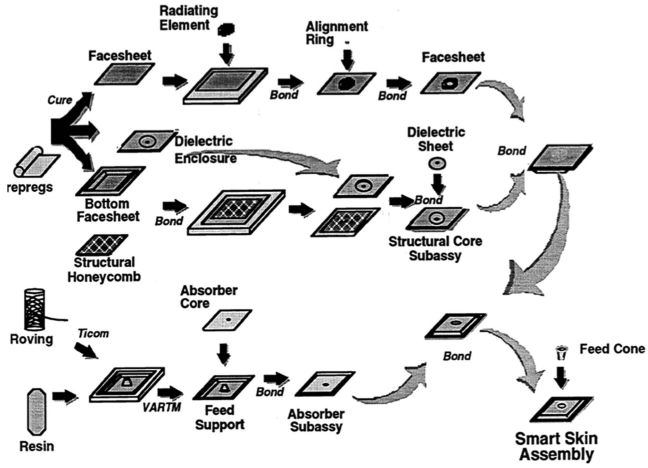

FIGURE 4. Smart skin RF element manufacturing process [5].

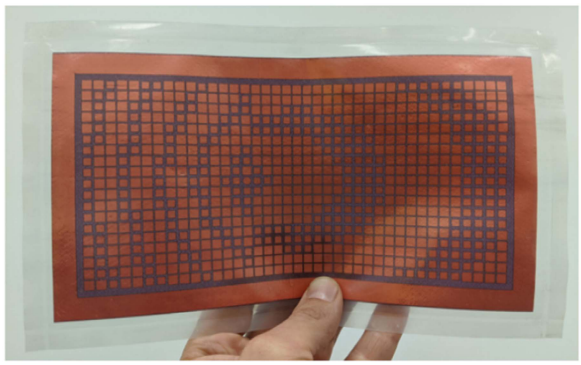

FIGURE 5. Laser profiled copper foil in uncured prepreg ply with a holographic pattern ready to be laminated in a composite structure [33].

For example, RF passive or active components may require metallic elements (such as conductive tracks, pins, or shapes) and other type of materials (like ceramic, quartz, glass, carbon fiber or sheets).

Frequently, various sensors or sensing platforms (like integrity monitoring systems) embedded into load bearing skins have also been explored. Often these examples use a combination of additive or subtractive manufacturing (3D printing, printing-additive, etching-subtractive) to alter the properties of the desired smart skin. In some cases, e-textiles are used to generate RF passive/active components. Various examples have been presented within the literature and are presented below in more detail.

A simplified composite single ring spiral antenna element is presented in [8]. The antenna is etched on an FR4 sheet which is bonded to one side of a NOMEX honeycomb layer giving it additional structural strength.

A carbon fiber reinforced plate is bonded to the back face of the NOMEX to support the whole structure. Similar manufacturing process were also used to manufacture a stacked patch antenna [9], [10], [11] and to house a microstrip antenna array [13].

Etching and printing techniques were used to fabricate arrays of patch antennas on three layers of RO4350 substrate [16], [17]. An etching technique was used to manufacture an antenna into the rib sections of a small UAV wing [20]. A smart wing was manufactured and presented by researchers in [23].

It was accomplished by embedding a dipole antenna which was also etched on to FR4 and embedded within a wing structure. Epoxy resin was used to bond the components together.

Direct writing of a Yagi-Uda antenna on structural elements of UAV skin is another method that was explored and discussed in [27]. The researchers used an inkjet printer to deposit conductive nanoparticle on the Kapton layer supported by epoxy/Kevlar skin.

A silver conductive epoxy EPO-TEK H20E was directly deposited on the composite panels and electroplated with copper to improve the RF properties of the antenna. Manufacturing process included printing of conductive ink, deposition of conductive epoxy and electroplating. Rigidity was defined by the strength of the fiber re-enforced composite backing. Advancements to this method include 6-axis direct writing of a metasurface antenna [55]. This work utilized an aerosol jet to deposit a silver seed layer on the conformal substrate. The seed layer was subsequently plated in copper to improve its RF performance.

Nicholson et al. [33] presented "continuous" and "discrete" holographic antennas patterns embedded into composite laminate structure (Fig. 5). The fabrication included: laser profiling of copper foil and lamination/transfer of the pattern onto uncured pre-preg. The laser profiling of the conductive elements was done using a Trotec Speedy Mark 700 fiber laser which cut think 25um copper foil while the dielectric was fabricated from 15 pre-preg plies of the Cytec Hexply 914E twill weave 48.0 g.m–2 S-Glass. The profiled holographic pattern was loosely held against a Teflon release film with an adhesive before being transferred to the consolidated pre-preg stack. The structure was finally cured in the autoclave according to the pre-preg manufacturer requirements.

The measured peak gains were 13.61 dBi for 'continuous' and 13.85 dBi for 'discrete' holographic antenna. The authors concluded that this manufacturing technique is fully compatible with existing aerospace manufacturing techniques and allow scalability of the manufacturing process. This process has since been extended to encompass truly conformal metasurface geometries in [157].

Axial mode helical antenna design and manufacturing was presented in [34], [37]. The antenna consists of the Co2Z hexaferrite-glass composite which was used as the laminate core with a helical radiator (in a 1mm copper strip) adhered to one side of the laminate with a copper ground plane adhered to the other side. This type of antenna is usually positioned inside the wing of a UAV. The antenna gain was pitch angle dependent and was shown to achieve a maximum gain of 0.541dBi at 2.39 GHz with an applied pitch angle of 10°. It was noted that a hexaferrite antenna, when miniaturized,

allows for more efficient use of space in UAVs. Manufacturing process consists of machining and cutting the copper ground plane and post bonding it to the composite core.

Lightweight materials are of primary importance in the design of load bearing antennas. Polymer based conductive inks have been used to print RF patches, dipoles and networks directly on polymer ceramic composite parts [39].

The researcher's used 200 um tall CNT sheet with 100 nm spacing between the fibers with a 1Ω/square resistance. They decreased the resistance tenfold by sputtering metal nanoparticle on the sheet. After integration with the polymer-ceramic structure, strong polymer-CNT bonding was observed. Manufacturing process involves CNT and polymer ceramic based ink printing of RF components directly on to UAV structures. E-textiles may also be used to fabricate load bearing components like antennas. The manufacturing process requires cutting conductive fabric to the required shape followed by attaching it to a ceramic composite fabric structure, infusing the structure with resin and bonding the entire structure together by curing it at the desired temperature [43]. The process of creating a lightweight planar antenna requires printing a calculated shape on a polymer-ceramic composite. After 12 hours curing it was noted that the conductive textile adhered strongly to a polymer-ceramic composite. Researchers concluded that this technology could be scaled up for mass production. Similar use of E-textiles and manufacturing processes have been presented in [44] and [45]. Authors in these papers used a 3D weaving machine to manufacture (weave) three-dimensional antenna structures in a glass fiber fabric creating three-dimensional orthogonal woven glass fiber/epoxy resin composite structure.

Modern embroidery machines and techniques allow the use of conductive yarns to fabricate elements of a patch antenna presented in [47], [48]. The fabrication procedure consists of sandwiching the following layers: reinforced fabric at the bottom, PDMS/ceramic composites in the middle and reinforced fabric on top. Conductive e-fibers were embroidered on the top and bottom layers of the polydimethylsiloxane polymer composite. Additional layers of PDMS/ceramic composites were added to achieve a 5 mm thick substrate which in turn created a conformal radiator for UAV applications.

An embroidery technique was also used to manufacture an ultra-wideband (UWB) amplifier [145]. The RF transmission lines were created by embroidery with conductive threads in the non-conductive substrate fabric. Three different stitching techniques were evaluated: (i) needle thread, (ii) needle and bobbin thread, and (iii) bobbin thread. A needle-bobbin stitch method was chosen for the manufacture of the UWB amplifier due to its reliability and less complexity compared to the other techniques. The conductive thread 100/34 DTEX 2ply HC from Shieldex was used to fabricate microstrip patterns on a HexPly 914E pre-preg. Two plies of copper mesh were used in addition to embroidery to create a ground plane.

The authors in [49] also used that same process to develop a load bearing small Egyptian Axe Dipole (EAD) antenna

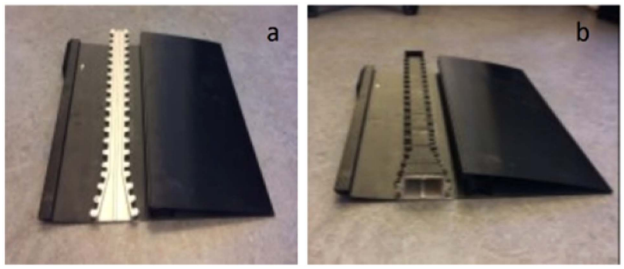

FIGURE 6. UAV wing with (a) split waveguide, (b) with waveguide [54].

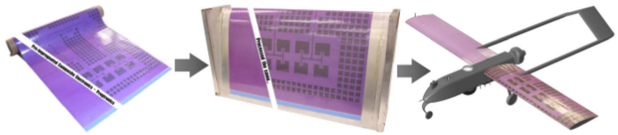

FIGURE 7. Composite material with printed EM traces [173].

embedded into an aerospace composite structure was manufactured and presented. Manufacturing process consists of the following steps: (i) preparing shape for embroidery (ii) embroider the antenna into S-Glass using bobbin stitch approach, (iii) laying up the materials to achieve the predesigned laminate thickness, (iv) impregnate with resin, (v) vacuum bag the structure, (vi) cure in autoclave at 180-200 ˚C, 700 kPa.

Use of non-woven veil materials to fabricate CLSS was discussed in [51] and [53]. The authors used a laser cutting machine to form the desired shape out of a carbon-nickel-copper veil. Following that, the sample was transferred to an Astroquartz II fabric and integrated with a composite structure by infusing it with resin and curing it in an autoclave.

Additive manufacturing techniques have also been developed for the fabrication of CLSS structures. For example, a Stratasys Fortus 400 mc 3D printer was used to manufacture an integrated waveguide and horn antenna [54]. The antenna was installed inside a 3D printed UAV wing (Fig. 6). Silver paint was used to achieve electrical conductivity along the waveguide. A measurement over the 7.5-18 GHz frequency range was performed in an anechoic chamber. The gain of the antenna embedded in the wing was, on average, 2.4 dB lower than the copper equivalent.

Another example using 3D printing technology in conformal load-bearing antenna structures (CLAS) applications was presented in [174]. The custom designed powder dispensing head was used to deposit a high permittivity powder onto a low-loss woven fabric based composite pre-preg material [174]. They used this method to manufacture the 3D composite structure by stacking together multiple layers with powder deposited on them. Authors concluded that the dry powder deposition method can be used to control anisotropic permittivity by varying the proportion of powder and the substrate.

A conceptual CLEE RF device was created as a part of the UAV's wing skin [173] (Fig. 7). The work focused on the impact of mechanical properties like tensile loading, biaxial loading and torsion/twist on the RF performance of a printed

~2.4 GHz patch antenna. According to the authors dynamic tensile loading, twisting and bending forces can produce a separation between the carbon veil (conductor of electromagnetic traces) and the composite structure resulting in a large shift with the resonant frequency of the antenna.

Multifunctional conformal load-bearing SWASS antenna was manufactured by interleaving S-Glass windows in CFRP pre-preg with ESA Teflon core [75] to [79]. Manual alignment and wrapping were used for manufacturing the waveguide antenna. Autoclave curing was used to consolidate the structures.

A similar process was used to manufacture the ground plane for a reconfigurable antenna. The ground plane was made from anisotropic CFRP composite cured in an autoclave while the radiating patch element was etched onto a Rogers 5880 substrate and bonded to the CFRP ground plane [85], [86].

Another example of fabricating smart structure is presented in [81], [82], where four plies of E-glass-fiber tissue were placed on both sides of the radiating element (cut from carbon fiber tissue and copper) and infused under vacuum with a liquid polyester resin.

Flexible flow sensing systems that utilize low-cost polyamide printed circuit boards have vast applications in micro UAV's. The authors of [92], [93] present manufacturing process and analysis of such system.

An etching technique is used to print the artwork for electronic circuits and sensing electrodes. Magnetron sputtering technology or pulsed laser deposition is used to deposit Cr/Ni and Pt on the sensing electrodes. After an annealing step and electric treatment, Parylene was deposited to encapsulate a sensor [94], [95]. Capacitive sensor array for aerodynamic pressure measurement and its manufacturing is presented in [96]. Standard 0.9mm thick PCB (rigid copper-clad glass-fiber) is used as a base to prove the concept. A rigid glass-fiber spacer was placed on the top and flexible copper-clad polyimide layer was used as sensing membrane. Layers are attached to each other by means of a 50-um thick adhesive tape. The structure was then attached to the prototype UAV wing [97] to [100].

The concept of using Fiber Bragg Grating Sensing Systems to monitor structural integrity of the wing of a helicopter blade is discussed in [110], [111], [112], [113]. Composite wing structures were fabricated from 10 layers of LTM45EL pre-pregs with Bragg grating fiber inserted into them using a vacuum bagging process. Smart skin antenna structure fabrication processes [115] discuss optimal placements of Bragg grated fiber strain sensors within this structure. They used an in phase compensation procedure for the antenna during its dynamic deformation. The fabrication process includes following steps: (i) manufacture the antenna array, (ii) adding the Bragg grated fiber sensing layer, (iii) bonding the sensing layer to the antenna array, (iv) aligning and laminating the face sheet and honeycomb, and (v) curing the sandwiched structure in an autoclave. The layers are bonded together using a vacuum bag/oven curing technique in the autoclave.

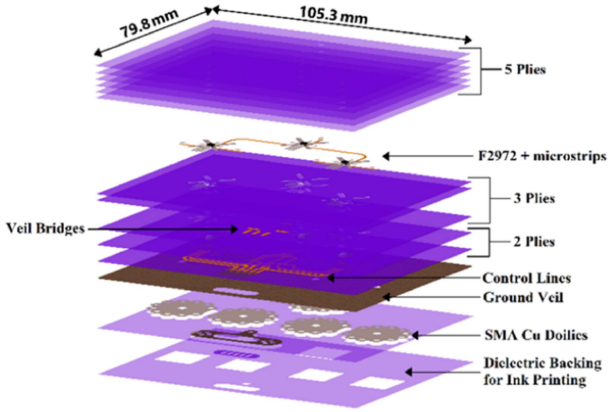

FIGURE 8. Multifunctional composite structure that includes microwave switching component networks [148].

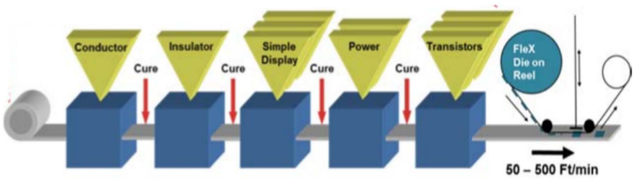

FIGURE 9. Flexible IC Hybrid Manufacturing Line [150].

Multifunctional Composite Structures for load bearing applications may include microwave switching component networks as presented in [144]. Composite structures consist of multiple layers of structural glass (S-Glass) material [148] as illustrated in Fig. 8. The conductive tracks were manufactured out of a mix of conducting silver ink and nonwoven carbon–nickel–copper (CNC) veil material.

A hybrid manufacturing approach was chosen to fabricate the structure. Firstly, the RF transmission lines and control circuitry components were transferred onto an uncured pre-preg. Then, once the laminate had been cured, silver ink was additively printed onto the back surface to create the remaining parts of the control circuitry. Follow-up work by the authors also described a more complex demonstration of an integrated FMCW radar front-end transceiver using a similar approach [179].

Advanced Conformal Load-Bearing Antenna Structures based on the flexible hybrid systems are discussed in [150]. High volume manufacturing for Flexible Hybrid Systems has been illustrated in Fig. 9. FleX^{TM} Silicon-on-Polymer^{TM} is a proprietary process to transform standard silicon wafers into flexible wafers. A FleX IC integration station is added in a roll-to-roll printed electronics line. Using this technique, the authors developed Flexible Hybrid System Prototype of the conformal load-bearing Antenna Structure.

Multifunctional structures with good microwave absorption performance and mechanical properties are presented in [167]. The authors provide examples of using CLAS for reduce radar cross-sections (RCS) applications.

TABLE 3. Manufacturing Processes

Manufacturing Process	*Ref No.*
3D Printing	[42], [53]
Composite Laminate	[27], [33], [34], [38], [40], [41]-[42], [44]-[46], [49]-[53], [69]-[79], [80]-[87], [110], [111], [113]-[116], [123], [126]-[128], [130], [138], [140]-[151], [157], [160], [161], [165], [166], [168], [173], [174], [179]
Composite Machining	[67]-[78], [83], [84]
Direct Write	[106]
Direct Write 3D Printing	[55], [144], [148], [150], [151]
Direct Write Thermal Spray	[35]
Elastomer Lamination	[39], [43], [47], [48], [124]
Embroidery	[49], [50]-[53], [145], [146], [149]
Laser Patterning	[51], [53], [55], [144], [147], [148], [157], [168], [179]
MEMS	[105], [106]
Metallic Structure Assembly	[28], [36], [37]
Polymer Metallization	[54], [55]
Optical FBG Lamination	[110]-[115]
Sandwich Structure	[9]-[12], [15], [125], [133], [135], [136], [158], [159], [164], [167], [170]
Screen Printing	[143]
Structural Cavity Only (Composite)	[131], [132], 137], [171], [172]
Structural Cavity - Internal Composite Sandwich Structure	[3]-[8], [13], [29], [162], [163]
Structural Lamination	[88]-[101], [118], [119], [121]
Traditional PCB	[14], [16]-[22], [24]-[26], [32], [36], [76]-[78], [85], [86], [96]-[101], [104], [105], [115]-[123], [125], [129], [169]
UV Curing	[164]
Vacuum/Sputter Deposition	[88]-[95], [164]
Vascular Channel	[40]-[42]
Weaving	[44]-[46], [126]

The authors designed and fabricated a 3D radar absorption composite hierarchical grid structure (3D-RACHGS) by molding metamaterials and using mechanical interlocking technology. The absorption performance was measured from 2 to 40 GHz, incident angles from 0° to 50° and exhibits an absorption bandwidth of 34.8 GHz and with an average absorption of 17.4 dB. It was concluded that the proposed 3D structure may be used in a new generation of multifunctional skins. Multiple manufacturing techniques were presented in this chapter. Manufacturing procedures are often defined by the materials that are used. Table 3 summarizes the manufacturing processes.

III. TESTING AND VALIDATION

The notion of load-bearing smart skins, in all cases, involves introducing some change to an aerospace structure. Typically, these can include material inclusions which can introduce material inhomogeneity or changes to the structure such as the use of cavities with a non-structural radome cover. In examples where dissimilar materials are introduced within a composite, this can result in unusual structural deformations due to varying stiffness or internal thermal stresses introduced during elevated temperature curing.

In some cases, there may also be the inclusion of holes or slots, such is the case for composite slotted waveguides [69] to [74]. Therefore, there is a need to better understand how all these aspects of aerospace smart skins change not only the mechanical properties but also the durability and integrity of the electrical systems being integrated. Some examples of structural testing and validation will be examined within this section including future challenges which still need to be addressed within the body of knowledge.

One aspect of using composite materials in aerospace applications is their susceptibility to damage. Damage to integrated smart skins can affect not only their structural performance but can have varying effects on their electromagnetic/electrical performance as well. Impact damage from foreign object debris (FOD) to a honeycomb sandwich structure with an embedded square aperture-coupled microstrip antenna was investigated in [125]. The inspection of the structure was carried out using non-destructive and destructive techniques (ultrasonic C-scan, X-ray radiography methods and physical cross-sectioning). The antenna return loss and radiation pattern were measured to determine a threshold of impact energy for which the antenna failed to function.

Another study focused on the influence of impact damage on a cylindrically conformal single and two element microstrip patch array CLAS [126]. This study also investigated the influence of the patch and array orientation relative to the cylindrical surface and noted that there was little change in the antennas before and after impact. In [127] and [128], the fatigue failure mechanisms of a copper trace embedded into glass/epoxy were investigated. The fracture of the copper foil conductor was observed at various levels of composite loading. No change in the overall characteristics of the stress vs strain chart were observed with the inclusion of copper foil. However, the foil did fail under cyclic loading. Specifically, copper failure was observed when the specimen was loaded between 25% and 75% of the glass/epoxy composite ultimate tensile strength (UTS). The crack growth in the copper was strongly related to debonding between the copper and composite. It was concluded that metals typically exhibit significantly lower fatigue life than glass fiber-reinforced polymer matrix composites as to be expected. The conductor failure is affected by both fatigue growth and ductile fracture which was shown in a detailed crack growth analysis [127].

A printed circuit board (PCB) fabrication of two narrow copper etched tracks was examined for its fatigue life in [129]. This process was proposed for multifunctional structures as it is made from a glass/epoxy composite material. The embedded copper traces exhibited robust behavior compared to those traces laminated onto the surface of the material [129]. The authors investigated the copper fracture mechanism and concluded that cracks were being formed on the composite surface which then propagated through the copper trace causing electrical failure.

In the development of the carbon fiber slotted waveguide antennas stiffened structure (SWASS), it was shown that the slot configuration influences the mechanical performance of the structure [130]. The results of finite element analysis (FEA) of seven single-slot designs showed that a 90° longitudinal slot was the best structurally by approximately 30%. Simulations have shown that the inclusion of five longitudinal slots required for array synthesis decrease the overall structural nonlinear limit load by 8%. Moreover, the experimental results indicated a 14% drop in the waveguide load limit. In [84] authors used ANSYS multi-physics analysis to compare both the mechanical and electromagnetic performance of a few types of CFPR slot antennas (log spiral, circular, and rectangular).

The proposed spiral slot antenna gave the most promising results. It was indicated that termination of the spiral slots with a sharp point significantly limits the static strength and fatigue endurance. The problem was overcome by using a semi-circular end slot termination. It was also concluded that the stress concentration for asymmetric slot geometries is sensitive to the relative angle between the slots and the main loading direction. The spiral slot compression test showed that filling the slot with epoxy resin results in a significant increase in the residual compressive strength of the samples. A good review of the SWASS development and mechanical modelling can be found in Chapters 3 and 4 of [175].

The weak points of dissimilar structures used in Load Bearing Skins are the interfaces between them. Authors in [152] carried out a study of interfaces between Carbon/Epoxy and Glass/Epoxy structures which underwent load under tension until failure occurred. Failures include delamination, ply rupture or resin pocket fracture. They discovered that when the different structures were connected together by an overlap multi-ply joint, their strength was close to that of a glass-fiber composite structure. In [153] the authors created a mathematical model to predict the failure in strength of Carbon/Epoxy and Glass/Epoxy hybrids employing various types of joints. An example of a load bearing antenna was examined in [154]. The carbon fiber and glass fiber composites T700/VTM264 and E-Glass/MTM57 were merged with differing lengths of overlap, before undergoing tension tests, with simultaneous crosshead speed, until failure occurred. It was concluded that applications would benefit from the presented types of joining techniques and predictive models provided by the authors in [153], [154].

It was also noted there could be a great improvement in ability to integrate structures like large radar apertures with the use of these overlapping composite structures without the addition of bulky and heavy structural supports.

Development of smart skin aerospace structures requires employing a co-design approach using both electromagnetic performance optimization and structural design processes. This hybrid simulation method was used to develop a new CLAS array for satellite communications [131], [132]. The designed antenna's structural properties were analyzed using FEA analysis carried out in NASTRAN and HYPERMESH. The structure loads were approximated for being from a typical reconnaissance UAV. The strain and deformation of antenna elements were optimized for the highest possible stiffness which was achieved using a grid structure. Moreover, it was also shown from simulation and mechanical testing (X and Y direction load and shear load) that the antenna deformation depends more on the antenna housing cavity design than the stiffness of the antenna radome [132] which forms part of the aircraft skin. Noting a similar design approach was presented in [13] to develop a CLAS. The electromagnetic and mechanical co-design process presented in this paper included three steps: antenna design, the antenna with added face sheet and honeycomb, and the entire structure full-wave simulation and optimization. The design was validated using electromagnetic and a mechanical three-point bend test.

Multifunctional aerospace skins can also be integrated with on-board electronic systems. This is related to the preparation of appropriate cavities for electronic devices within a structural skin. Typically, these result in a degradation of a structure's load-bearing capacity however it can increase the structures functionality. In [133], various types of filling materials were investigated to improve the stiffness of carbon/epoxy sheets with polyurethane foam sandwich structures. These cavities were used to house electronics systems. A flexural four-point bending test indicated a recovery of 87% of the structure stiffness when the cavity was filled with high density (90.1 kg/m^3) expandable form.

Integrating electronics with multifunctional aerospace skins require veils or woven/embroidered tracks or patches to interconnect them. Nicholson et.al. [168] manufactured and performed 4-point bending tests of the fiberglass laminate containing either embroidered or nonwoven veil microstrips. The veil based microstrips were superior in mechanical deflection performance to the embroidered ones. It was also concluded that the maximum flexural stress (at failure) of a veil based microstrip was worse in comparison with a straight laminate microstrip by 90 MPa.

A. FUTURE CHALLENGES IN MUTLIFUNCTION TESTING AND VALIDATION

The ad-hoc approach to testing and validation of CLSS in the reviewed literature is likely in response to the difficulty of merging both mechanical and electromagnetic testing setups. If CLSS is to be widely adopted, then development of multi-physics testing regimes will be necessary.

Mechanical validation as an example, has a number of predefined standards used to understand different aspects of the mechanical properties of a material. These typically include:

1) Tensile testing – in-plane tensile testing of composite laminates is the most common test performed on composite materials with tests standards (ASTM D3039, EN 2561 and ISO 527-4/5).
2) Compression testing – where specimens are either parallel sided with a short, unsupported gauge length to prevent buckling (ASTM D695, ASTM D3410, ASTM D6641 and ISO 14126).

3) Shear testing – the interlaminar shear strength test (ILSS), or short beam shear (SBS), uses a small specimen loaded in a three-point bend configuration (ASTM D2344, EN 2563 and ISO 14130).
4) Compression after impact (CAI) testing – assess damage to composite laminates with internal delamination (ASTM D7136, ASTM D7137 and ISO 18352).
5) Fatigue testing – Cyclically loading of the laminate to induce localized fatigue (ISO 13003)

Within the reviewed papers, these standards have been extensively used to validate Finite Element Analysis (FEA) models of multifunctional structures. However, mechanical testing only forms one part of what is required to validate CLSS. In many of the reviewed papers, simultaneous testing of the multi-functional aspects of the proposed CLSS's does not occur. This multifunctional testing is important to identify the complexity of CLSS's (such as those explored in [173]). This can occur not only due to the deformation of the parent structure but also the local strain around the radiating elements. In some cases, it is observed that multifunctional testing is difficult to achieve or difficult to interpret key aspects of the measured results. This review has identified that a standardized test and validation process is needed to help identify some of the key design considerations needed to improve CLSS.

IV. APPLICATIONS

From the previous section it has been shown that there are numerous manufacturing processes and materials that have been utilized for CLSS. This section explores some of the different CLSS applications which have been reported in the literature. Moreover, it gives an overview of the three main categories of CLSS which include antennas, electronics, and sensors.

A. ANTENNAS

One of the most prominent areas researched in CLSS is antennas. This area forms much of the literature due to the large acceptance of electromagnetic communication and sensor systems used within the aerospace sector. Hence, there is a natural synergy in being able to use structures to radiate electromagnetic fields. The primary goal of CLSS antennas (or as they are more commonly known as conformal load-bearing antenna structures (CLAS) or conformal load-bearing antenna array structured (CLAAS)) is to identify radiating topologies which are suitable to be integrated directly into conformal composite skins. The overall aim is to replace traditional aerospace antennas (such as blade monopole antennas and slotted waveguides) with alternatives that both reduce parasitic drag and weight of a platform. Hence, this results in fuel or energy savings and contributes to reducing the overall operational life-cycle costs of a platform [1]. Examples of antennas include planar antennas, leaky wave antennas, and highly integrated 3D and waveguide antennas. An overview of these technologies will be discussed within this section.

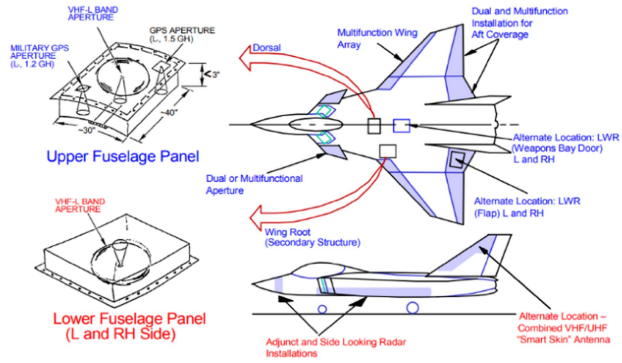

FIGURE 10. CLAS location on an airplane [7].

Planar Antennas: Over recent decades there has been a significant number of publications dealing with aerospace smart skin designs which have focused primarily on planar antenna technologies [3], [4], [5], [6], [7], [8], [9], [10], [11], [12], [13], [14], [15], [16], [17], [18], [19], [20], [21], [22], [23], [24], [25], [26], [27], [28], [29], [30], [31], [32], [33]. Planar antennas of various topologies have been explored. These are typically constructed using thin sheet conductors (printed or laminated) on or in a dielectric substrate. Due to their overall thickness and suitable bandwidth compared to traditional aerospace blade monopole antennas they are well suited for CLAS applications [3]. This is especially the case when dealing with composite based structures where dielectric structural composite materials (i.e., ceramic, glass, polymer and/or quartz fabrics) can play the role of the RF substrate. However, to date planar antennas have focused mainly on the development of antennas using traditional radio frequency (RF) materials and processes while focusing on integration using structural cavities and radomes. Typical Smart Skin panel locations on an airplane is illustrated in Fig. 10.

The first example of a CLAS to be examined is a wideband (150 MHZ to 2 GHz) antenna [4], [5], [6], [7]. The achieved bandwidth was realized in this design utilizing a unidirectional, multi-arm, cavity backed spiral antenna embedded in a load-bearing composite sandwich structure. It was embedded in the fuselage skin of a multi-role fighter. The antenna construction considered the operational conditions of the platform, such as its lightning susceptibility and repairability. The CLAS was designed to operate with various aircraft systems such as: communication, navigation, identification as well as electronic warfare payloads.

Another example of a load-bearing spiral antenna operating over a similar frequency range was described in [8]. The antenna was fabricated on a single-side FR-4 substrate and consisted of a multilayer structure including a cavity absorber and carbon fiber reflector. This antenna was designed for integration within an aircraft wing. The examination of a broad bandwidth stacked patch microstrip antenna integrated into a multilayer sandwich structure has also been presented in [9]. The sandwich construction consisted of two composite face

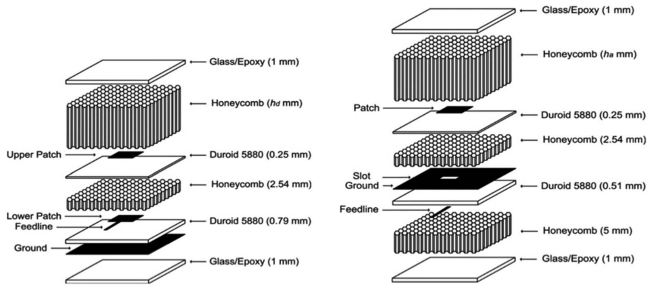

FIGURE 11. Layer composition of a CSS [9]; Left Direct-feeding stacked patch antenna; Right Aperture-coupled patch antenna.

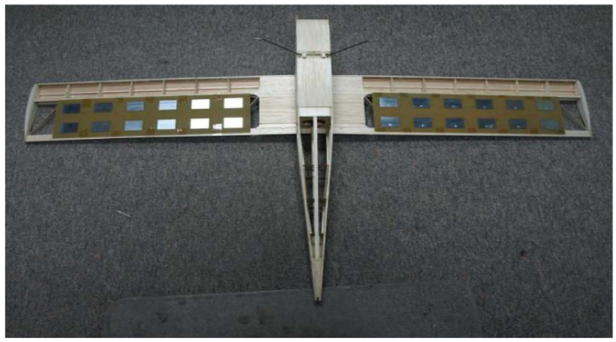

FIGURE 12. Fabricated CLAAS antenna boards attached to the bottom of the UAV wing [18].

sheets separated by a NOMEX honeycomb core. The patch radiating elements were fabricated on Rogers Corporation Duroid 5880 substrate and bonded to the top and bottom of the composite sandwich structure (Fig. 11).

The CLAS operated over a frequency range of 11 GHz to 12.75 GHz with a gain of approximately 12 dBi. Similar CLAS's were investigated in [10] and [11].

There have also been several investigations into planar antenna arrays [12], [13], [14], [15], [16], [17], [18], [19]. In [12], [13] a four-element patch CLAAS was investigated. It is also worth mentioning that in [12] the authors reported the use of an inversion method to analyze the effect of flaws in the bond layer between their patch array and a honeycomb layer which forms part of a load-bearing radome. An alternative array method was proposed in [14]. This example introduced a new type of pixel antenna. This antenna used microelectromechanical systems (MEMS) switches to enable reconfigurability. This antenna was able to achieve operating frequency bands at 1.5 GHz, 2 GHz or 3.1 GHz, with the gain of 5.3, 3.7, and 5.1 dBi, respectively. This antenna was also tested under bending load with no noted degradation in its performance. A linear polarized phase array microstrip antenna was presented in [15] with a center frequency at 7.5 GHz and a realized gain of 17.23 dBi. This array was designed with a full 1-dimensional electronic steering network which could steer the main beam to ± 45 degrees. The patch elements were formed within a honeycomb sandwich structure which consisted of 8 patch elements. Similarly, 12 and 14 element planar patch arrays were reported in [16], [17], [18]. These arrays were embedded in an unmanned aerial vehicle (UAV) wing (Fig. 12).

The antennas operated in the ISM band with a center frequency of 2.45 GHz and were fed by a controlled combiner/splitter network. That configuration allowed for UAV communication improvements by enabling steering in both azimuth and elevation to track the position of a base station. Finally, a circularly polarized, circular antenna array was investigated in [19]. The four-element patch antenna system was designed to be installed conformally around the surface of a UAV fuselage. The array with an omnidirectional radiation pattern operated at the frequency of 5.6 GHz with the gain of 5 dBi.

An alternative method to developing a load-bearing antenna structure was investigated in [20], [21], [22]. In [20], the authors compared the performance of a straight, "L" and "T" shaped printed monopole antenna elements that were embedded as wing ribs in a small UAV. The antenna elements were designed to operate in the 2.45 GHz frequency band for use with wireless local area networks (WLAN). The best performance (maximum gain of 1.4 dBi and return loss of -20 dB) was obtained for the "L" shape monopole. Due to the element's radiation characteristics, it was investigated in a 4 – element and 8 – element array [21]. In [22], the authors studied an increase in the communication range and data throughput of WLAN link between a UAV and its base station.

Conformal antennas can also be designed to fit existing antenna locations on airframe structures with minimal modification. The authors in [23] described a method of replacing a traditional monopole blade antenna with a planar annular slot radiator, as well as a technique of embedding a dipole antenna into a UAV's vertical stabilizer. The slot antenna was able to be designed to fit into an existing recess created for a blade antenna. The new antenna was then covered by a thin radome. On the other hand, the dipole was bonded to the surface of the vertical stabiliser. The overall performance of both antennas had little effect on the vehicles communication system. In both cases they showed similar radiation patterns, polarization, and maximum gain at or near the horizon. Another example of a thin CLAS, S-band, annular slot antenna molded into a carbon fiber reinforced polymer (CFRP) composite structure of a UAV was also presented in [24]. This example provided a better approach to the integration of the CLAS as the cavity antenna was much thinner than previous examples.

Steady progress in CLAS has allowed the design and integration of popular UHF radiators such as meander lines [25], log-periodic [26] and Yagi-Uda arrays [27] into flying platforms.

These examples have utilized several different dielectric materials where the radiating elements have been fabricated using copper foil adhered on a dielectric base layer of CRI-0512S (DuPont) [25], popular glass-reinforced epoxy laminate FR-4 [26] or directly printed on Kevlar/epoxy composite

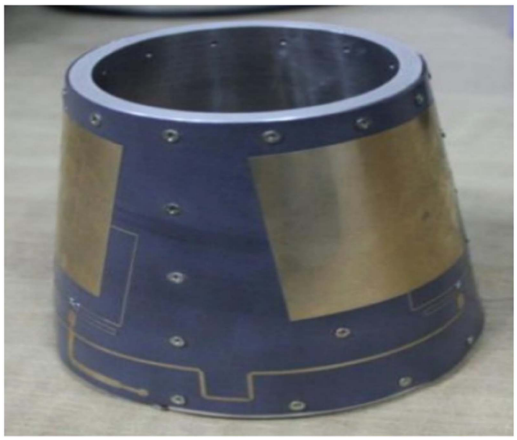

FIGURE 13. Prototype of a CLAAS missile-borne conformal navigation antenna [31].

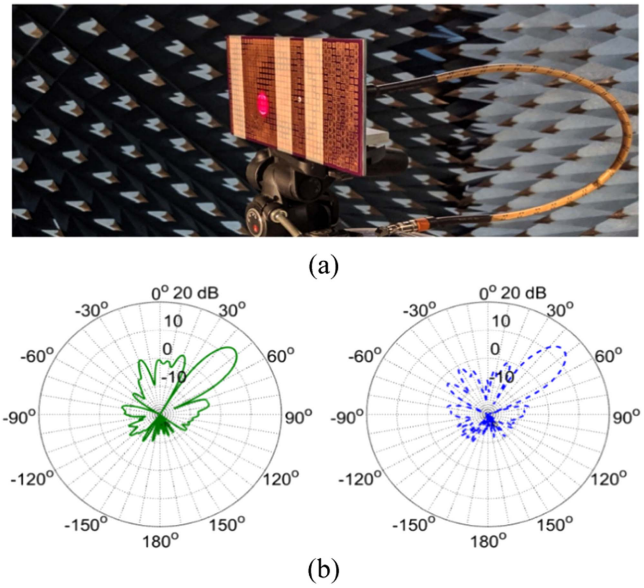

FIGURE 14. (a) Measurement configuration, (b) Measured realized gain at 10 GHz for the "continuous" (LEFT) and "discrete" (RIGHT) holographic antennas [33].

panels using silver conducting ink [27]. Another example of UHF CLAS was presented in [28]. The large patch antenna was designed to conform to the belly of a cargo helicopter. The antenna resonated at 480 MHz with a peak gain of 6.7 dBi. An interesting design of a double band (UHF and L – band), sandwich structure CLAS was reported in [29]. The radiating element of the antenna also included a log-periodic slot that was inserted into the magneto-dielectric material. The antenna was installed within the air speed brake of a KT – 1 trainer aircraft.

The possible applications of planar CLAS have not been limited only to aircraft or unmanned aerial vehicles. In [30] and [31] the authors reported the development of missile-borne dual-band conformal microstrip patch antenna arrays. The arrays showed omnidirectional radiation in the horizontal direction, and they operated over three global navigation satellite system (GNSS) frequencies of 1.575 GHz (GPS L1), 1.562 GHz (Beidou-B1) [31] (Fig. 12) and 1.268 GHz (Beidou-B3) [30]. The example is illustrated in Fig. 13.

The idea of using the skin of a UAV for a reconfigurable antenna was investigated in [32]. The principle of the antenna was based on the theory of characteristic modes for an electrically small conducting body. In the case where the skin of a small UAV is manufactured from a conducting material, a small voltage or current probe adjacent to the conductive surface can excite currents to flow over the structure. Consequently, the UAV's skin can become the electromagnetic radiating aperture. The probe's arrangement allows for the control of the current distribution and thus, antenna radiation pattern. In the development prototype, two small monopoles and an inverted F-shape patch probe was used to excite the skin of a small UAV model at UHF 800 MHz. It was demonstrated that the three-port excitations allowed for the control of the radiation pattern. The antenna achieved a realized gain for the broadside, forward, and aft beams of 3.31, 0.14, and 5.07 dBi, respectively.

There has been noticeable progress in the development of conformal, metamaterial - inspired antennas. Two examples of composite embedded, load bearing, high gain, metasurface holographic antennas were presented in [33]. This type of leaky-wave antenna was design using an artificial impedance surface (AIS) where the radiating pattern was controlled using holographic principles. Two fabricated CLAS examined the differences in using a continuous and discrete holographic pattern at an operating frequency of 10 GHz. The main beam in both examples was designed to radiate at an elevation of 45 degrees and they achieved a realized gain of 13.61 dBi and 13.68 dBi, respectively.

Significant steps in the development of antennas were presented in [33] where the authors designed, and compared two meta-surface 10 GHz antennas with two types of inclusions: using a conventional hexagonal grid with continuous space distributions and a Voronoi partition with constant gaps between inclusions. Measurement setup is illustrated in Fig. 14.

It was noted that both antennae displayed similar properties like gain, surface impedance, insertion loss and radiation efficiency, however the standard hexagonal grid was limited to a 2D dimension while the Voronoi partition structure was suited for conformal surfaces. The antennas were fabricated using a process compatible with standard glass fiber composite manufacturing. This work has since been extended to conformal surfaces with both convex and concave geometries [157].

Interesting concepts for embedding the reflector backed printed dipole antenna to the shape of a typical wing leading edge are discussed in [162]. The antenna was developed for UAV applications. The printed dipole antenna was encased in a glass fiber reinforced polymer (GFRP). The gain of the fabricated antenna was 5.22 dB across a 1.66% measured bandwidth from 3.580 GHz to 3.638 GHz. The 3 dB beamwidth in the H-plane and E-plane was assessed as around 700 and 900 respectively.

FIGURE 15. Ice penetrating antenna [165].

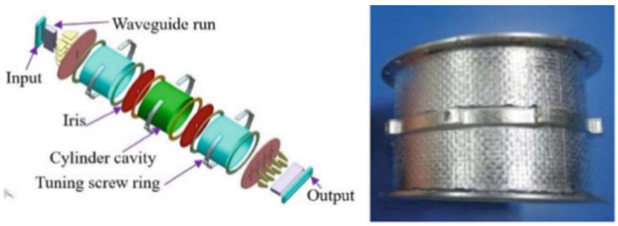

FIGURE 16. S band cavity filter (components view Left, Assembled view Right) [171].

Airborne radars are effective tools in monitoring polar ice critical regions (such as temperatures of mountain and outlet glaciers). Egyptian Axe Dipole (EAD) [165], [166] is presented as being used to sound polar ice and image temperatures of glaciers (Fig. 15). This type of a near-high frequency antenna was designed for UAS systems, like helicopters. The antenna center frequency is between 30 MHz and 40 MHz which reduces the effects of scattering and improves the reduction of clutter.

Inverted-F antenna (IFA) is used in mobile communications due to its small size, its lightweight and low profile, and simple structure. A phased array antenna skin is proposed in [158]. PIFA (Planar inverted F antenna) is used as a radiation element. Each element of the array has an omnidirectional radiation pattern and low profile. The PIFA element is integrated within the wing of an aircraft using composite materials. The use of multilayer composite materials allows the structure to perform as a load bearing element. The gain achieved was between 21.3 dBi and 19.2 dBi and the bandwidth was between 5.3 and 7.6, for a scanning angle between 0° and 135°.

Some aerospace antennas use lightweight bistable composite structures [170]. These structures are deformable in nature, and they are used as mechanical arrangement mechanisms. They can maintain two stable states and can switch between them. The authors present a UHF band bistable monopole antenna operating at 0.42 GHz when folded and 1.2 GHz when unfolded. The antenna may be set to directional or omnidirectional mode of operation depending on whether it's folded or unfolded. The antenna uses copper foil, carbon fiber and glass fiber as the substrate. The best impedance matching was achieved by laying the copper foil inside the GFRP. The layers are fused together by curing them into one structure.

At present, there is a high level of interest in using satellite links for communication, broadcasting, navigation, etc. The S Band Radio Frequency (RF) Cavity Filter developed and tested in [171] used carbon fiber reinforced polymer Fig. 16. This strictly tuned cavity structure passes wanted frequencies and blocks undesired one.

The study utilized CFRP for fabrication of a filter destined for communication satellites. Measured values of main RF parameters like return loss, insertion loss and frequency drift were 13 dB, 0.9 dB and 0.7 MHz, respectively. RF tests concluded that insertion loss varied from 0.6 to 0.9 dB as temperatures raised from ambient to 125 °C. Return loss of 20 dB was noted in ambient conditions, while a return loss of 13 dB was noted at a temperature of 125 °C. Observed frequency drift was up by 0.7 MHz (from center frequency) at a temperature of 125 °C. It was concluded that a CFRP-based cavity filter design could meet both structural and RF requirements while also providing large weight saving and thermal stability.

The presented examples on planar antennas have illustrated that they are well suited for CLAS applications. In most of the presented examples there is a clear trend in not only using traditional planar antenna topologies but also taking advantage of traditional manufacturing approaches such as the use of commercial RF substrate materials and chemical etching processes. The load-bearing aspects of the CLAS are typically formed by the inclusion of a structural cavity or the use of a transparent load-bearing radome. In the latter examples there is a clear push to examine how different composite materials can be used to form both the radiating elements and ground plane structures. This indicates that antenna CLSS are progressing towards a higher level of integration compared to the earlier demonstrated works.

3D Antennas Topologies: The research on the development of CLAS has not been limited to planar antennas. Successful attempts to integrate conformal antennas on a 3D surface have also been examined however, to a much lesser extent. One of the reported designs was a two-element miniature axial-mode hexaferrite helical antenna for UAV communication applications [34]. The antenna operated at the frequency of 2.44 GHz with the realized gain of 2 dBi. A reduction in the antenna array size was achieved through a design based on a Co2Z hexaferrite glass composite core. Global Navigation Satellite System (GNSS) bifilar helix antenna for use in UAS applications was described in [35]. The wideband (1.6 to 1.95 GHz) antenna was fabricated on a polyetheretherketone dielectric rod. The radiating element of the device was developed with copper using a Direct Write Thermal Spray (DWTS) technique. The antenna was installed inside the vertical stabilizer of the Dakota UAV. NASA reported the development of three ultra-lightweight antennas compatible with High Altitude Long Endurance Unmanned Aerial Vehicles (HALE UAVs) [36].

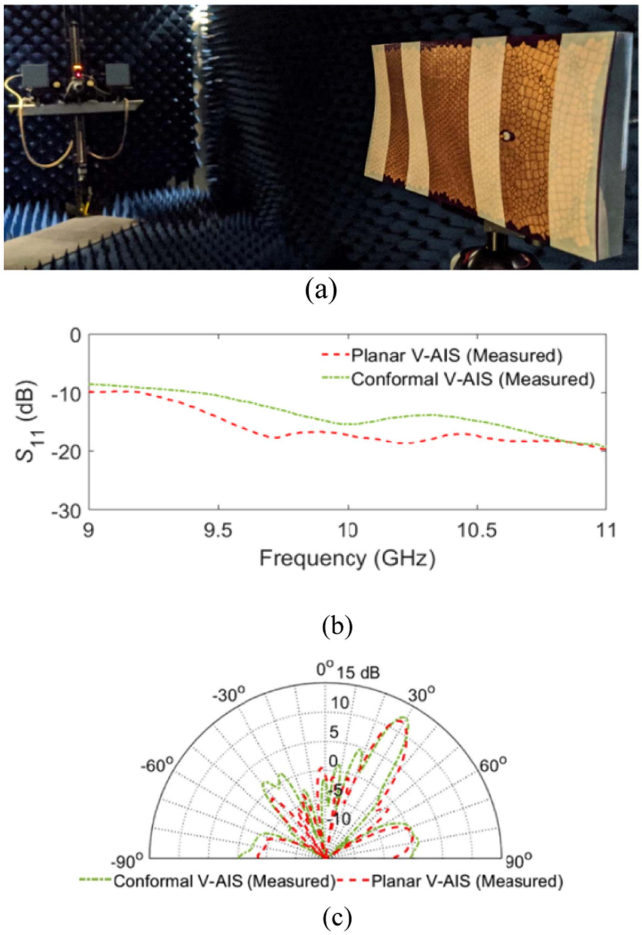

FIGURE 17. (a) Measurement configuration V-AIS; (b) Measured S11 for the conformal and planar V-AIS ; (C) Measured realized gain at 10 GHz in the E-plane [157].

As part of this project, a wideband helical antenna, balanced antipodal Vivaldi antenna and reduced surface wave antenna were proposed. All antennas were embedded into the UAV's wing structure. Other examples of three-dimensional conformal antennas adapted for installation on the surface of the UAV's body are described in [37] and [38].

These two examples included UHF antennas based on the common dipole [37] and monopole [38] topologies. These were designed as low-profile antenna manufactured using strips of copper sheet incorporated into a structure. High-precision satellite reflectors use honeycomb composite structures [159].

They may differ depending on materials used, reflector configuration, thermal deformation of the structure, etc. The authors dwell on making the structure "*lighter, larger, more refined and more stable*". The authors consider 3D manufacturing technology and functional requirements of future satellite antenna reflectors.

The authors in [157] demonstrated a metasurface antenna on an arbitrary conformal surface photographed in Fig. 17. The measured performance of the antenna agreed with the simulated results. The unique manufacturing approach can incorporate large-scale conformal metasurface arrays on arbitrary geometries. It is predicted that such antennas will cover significant regions of a platform's exterior surface of the UAV, thereby significantly enhancing its communications or sensing capabilities. It was concluded that this work was the next step in the deployment of truly conformal multifunctional composite structures.

Two manufacturing methods to fabricate a conformal metasurface antenna on a UAV are presented and compared in [55]. The researchers designed an antenna that exhibited a pencil beam radiation pattern at 10.0 GHz. The first manufacturing method utilized a 3-axis Trotec fiber laser to etch the flattened metasurface geometry in copper foil which was then stretched over the UAV fuselage. The second approach utilized a 6-axis nScrypt to print the metasurface pattern directly on the doubly curved surface of the UAV fuselage [55]. The authors concluded that the discussed manufacturing techniques are cost effective and can produce antennas with comparable performance.

Carbon fiber waveguide antennas: CFRP is playing a vital role as a structural material for the manufacture of modern day and future platforms in the land, sea, air, and space domains. Carbon fiber (CF) is made from long graphitized polymer strands which produce favorable mechanical properties and are electrically conductive. The conducting feature of the material is attractive for CLSS and antenna applications. However, the conducting mechanism of CFRP is strongly dependent on the composite fabrication process. More specifically, bulk conductivity of a laminate may have varying conductivities due to the anisotropic nature of carbon fibers [56]. CF for CLSS applications is typically described in three distinct forms which include uni-directional fabrics, woven fabrics, and non-woven veils.

Uni-directional fabrics are created from tows of CF (bunches of individual fibers). These tows are all laid in parallel next to each other to create a long sheet of material. Unidirectional fabrics are usually stacked in various orientations to create mechanically quasi-isotropic CFRP laminates. These laminates are highly anisotropic in their conductivity due to the parallel direction of the CF in each layer. Current is only able to flow efficiently in the direction of the fibers while the two orthogonal directions can be highly resistive.

Woven fabrics are created using traditional textile weaving processes. This involves using CF tows as the base strands for the weaving process. The tows are then woven in the warp and weft directions to create different fabric patterns such as plane, crows-foot, twill, and satin for example. These fabrics typically conform well to complex curved geometries and are more quasi-isotropic in their electrical properties compared with unidirectional CFRP. This is due to fibers running in both the warp and weft directions.

Finally, the non-woven veil materials are made of short CF which are held together using a weak binder. As the name suggests the fibers are randomly orientated and can be manufactured to have different areal densities. The electrical conductivity of these materials is more isotropic compared

to uni-directional and woven fabrics due to the random placement of the fibers however their conductivity varies greatly based on the areal density.

The conductivity of CFRP behaves slightly differently from the conducting mechanism which governs well known isotropic metallic conductors. Although the conductive carbon fibers are typically stacked and laminated into thick panels, the inclusion of the epoxy resin matrix partially isolates neighboring fibers. This process reduces the contact area between each of the fibers and hence decreases the overall ability of CFRP to carry direct currents (DC) and low-frequency alternating currents (AC). As the frequency increases, this inhibiting feature reduces because of the high capacitive coupling between fibers. The conductivity of CFRP increases with frequency up to the microwave range where both the skin and proximity effects start to adversely affect its electrical properties. That unusual behavior in CFRP has driven researchers to better investigate its electrical properties.

The conductivity characteristics of carbon fiber composite were determined through investigating its shielding effectiveness (or electromagnetic transmission and reflection properties). At HF frequency ranges, a two-loop antenna technique has been used to investigate this property [57]. In contrast, the shielding effectiveness of CFRP within the microwave region has been measured using both a free space reflection/transmission [58] and rectangular waveguides techniques [59], [60], [61]. These techniques have shown that there is a strong correlation between the orientation of carbon fibers in composite multilayered structures and the resultant anisotropic or quasi-isotropic electromagnetic properties [59], [62].

The conductivity of CFRP has also been analyzed using DC surface resistivity measurements [63] and wideband analysis of its attenuation using microstrip transmission lines [64]. In [65], a method to extract the conductivity of carbon fiber from the loss associated with a CFRP monopole antenna was proposed. It has been shown within the literature associated with analyzing the electrical properties of CFRP that the conductivity varies with frequency, material thickness, fiber direction or weave and to some extent the measurement method applied.

The conductivity of CFRP has been reported at values which lay between tens to hundreds of thousands of Siemens per meter (S/m). This value is much smaller than copper-based conductors and shows that CFRP can be treated more like a lossy conductor. To overcome this loss associated with CFRP, metallization methods can be applied to improve its performance. In [66], the conductivity was improved by metalizing the inner surface of a CFRP waveguide with copper foil, conductive paint, and a metalized carbon fiber veil. The results of this work illustrated that a thin layer of metallization can significantly improve the performance of CFRP waveguides.

The Slotted Waveguide Antenna Stiffened Structure (SWASS) concept has been extensively investigated [67], [68], [69], [70], [71], [72], [73], [74], [75], [76], [77], [78], [79]. The manufactured test example is illustrated in Fig. 18.

FIGURE 18. Manufactured test fixture with slotted cover plate [77].

There are two types of slotted waveguide antennas. The first type of antenna is based on the principle of standing waves. In this structure a waveguide antenna consists of a standard rectangular waveguide which is shorted at its end to create an internal standing wave. For this type of antenna, the waveguide behaves as a high-Q resonant cavity. The waveguide radiates electromagnetic energy through small slots positioned at locations where the maximum filed strength for the standing wave occurs. This is typically at a half-guided wavelengths for the desired operating frequency. In the travelling wave type of slotted waveguide antenna, the electromagnetic field moves from the input to the terminated output of a waveguide. The antenna radiates from slots located at an arbitrary position along the waveguide except for the central waveguide plane. The slot position is determined by the required parameters of the antenna and its radiation pattern.

Waveguides operating at microwave frequencies have similar dimensions and shapes to top-hat stiffeners that are used as reinforcements in aerospace structural skins. This feature makes SWASS a highly desirable candidate to be integrated into flying airframes. It covers all aspects of CLAS including lowering weight and removing drag penalties that are present with current aircraft antennas. It has been shown that the performance of CFRP SWASS is almost equivalent to traditional metallic antennas.

In [70], the comparison of a X-Band slotted waveguide antenna manufactured from aluminum and CFRP was investigated. The authors noted the only difference between the two antennas was a 2 dB reduction in the antennas gain caused by the Ohmic loss of CFRP (Fig. 19).

It has been noted that one of the main drawbacks to SWASS is a degradation in its load-bearing capacity which is caused by the introduction of the radiating slots. This problem can be addressed by shortening the length of each slot however, this negatively impacts its performance. In [71] and [72] the authors described a novel method to reduce the slot length. The novel approach to SWASS is illustrated in Fig. 20.

Despite the modification, the antenna realized gain remained at a similar level to a full-length slot. This was

FIGURE 19. Photographs of the aluminum (left) and CFRP (right) 10-slot slotted waveguide antennas (SWASS) [70].

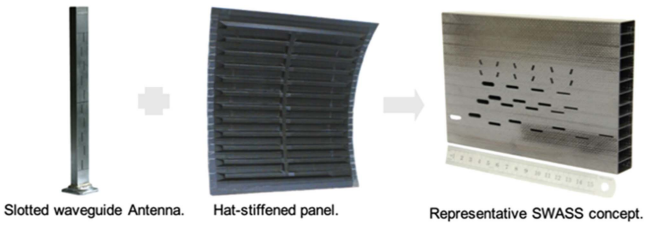

FIGURE 20. The SWASS concept presented in [72].

achieved by loading the slot with a split-ring resonator (SRR). However, this introduction affected the antennas reflection coefficient due to the large cross-section of the SRR. This problem was resolved by substituting the SRR with a wire element capacitively coupled to the waveguide broad wall [73]. This improved the antenna's gain and reflection coefficient while allowing for the reduction of the slot length. It was shown that the slot length using this method can be significantly reduced (approaching a quarter-guided wavelength) while maintaining identical radiation characteristics. Furthermore, investigations in [152], [153], [154], [155], [156] illustrated that the strength of SWASS could be further improved by adding interleaved glass dielectric windows over the slots. The authors investigated several different interleaving patterns and showed that it was possible to recover up to 80% of the original structural strength. This method along with the introduction of the capacitive wire element show that there are several viable solutions to solve the mechanical issues with SWASS.

Feeding of a CFRP waveguide must also be considered as they suffer from poor launching and feeding transitions when using traditional waveguide launching methods. This is caused by a thin layer of epoxy which insulates the CF walls of the waveguide. Along with this, CFRP cannot be soldered or braised like traditional metallic waveguides and new methods are required to make a good electrical connection to metallic waveguide flanges and feeding adapters. In [74], a loop-type end-launcher was explored to feed CFRP waveguides. The developed launcher did not require grounding to the broad wall of the waveguide. A method for feeding an array of travelling wave SWASS was also presented in [75].

As SWASS belongs to the CLAAS sub-category of CLSS, the orientation of slotted waveguides and hence the antenna scan plane is constrained by typical aerospace structures. This is because the orientation of CFRP stiffeners is primarily dependent on the mechanical load applied to the structure (i.e., hat stiffeners always run longitudinally in a fuselage). The concept of a beam steerable SWASS was presented in [76] to overcome this issue.

The beam steering mechanism was accomplished using dispersion engineering of the traveling electromagnetic wave. The proposed structure was based on the theory of composite right- and left-hand transmission lines (CRLH-TL) used to advance or delay the phase between each slot in the array. The phase shift control was realized by incorporating varactors and an inductor loaded transmission line into a waveguide. The radiation pattern was electronically controlled by changing the varactor biasing voltage. The fabricated antenna exhibited a maximum beam scan angle of ± 11 from broadside with peak a realized gain in the range of 3.6 to 4.3 dB [77].

The design was later improved by separating the DC tuning circuit from the waveguide structure. This allowed the tuning structure to be directly integrated within CFRP SWASS [78].

Optimization and analysis of slotted waveguide antenna structures were performed in [172]. The authors assessed and optimized the use of a SWASS antenna in an X-47B unmanned combat aerial vehicle designed by Northrop Grumman. The panels were used as a weather radar operating in X-band (10 GHz) frequency. Optimization takes into account minimizing the mass of the panel and maximizing the buckling load while operating frequency stays as close as possible to 10 GHz.

Other Carbon Fiber-Based Antennas: The reinforced, continuous carbon fiber (RCCF) composite ultra-wideband (UWB) monopole patch antenna was presented in [80]. The RCCF composite conductivity was enhanced by adding a small fraction of multiwall carbon nanotubes to the epoxy matrix. Other investigations have focused on planar carbon-fiber composite wideband radiators including the lozenge monopole antenna designed for frequency ranges below 4.5 GHz [81], [82] and an X-band slot equiangular spiral (log-spiral) antenna [83]. An interesting X-band CLAS design was reported in [84]

(Fig. 21). The authors developed a cavity backed CFRP slot antenna equipped with a capacitive feed that did not need direct contact with its feeding coaxial line and the antenna radiating element which was embedded into an epoxy resin.

The CFRP antenna was compared to an equivalent metallic slot antenna, and it was showed that both antennas had

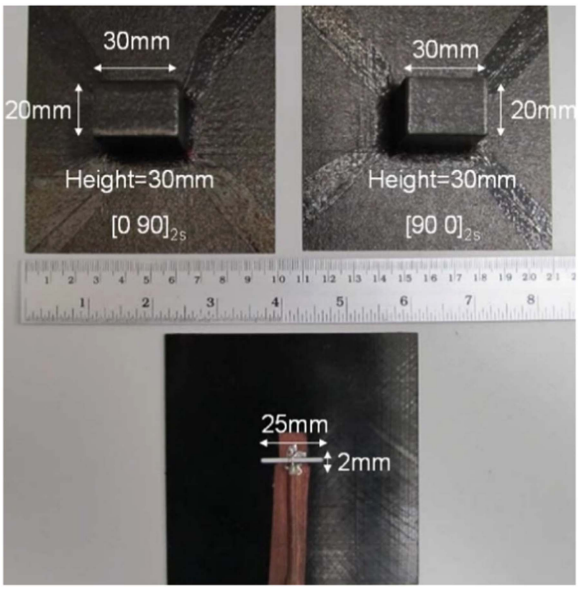

FIGURE 21. CFRP slot (lower) and large cavities presented in [84].

similar radiation performance. In [85] and [86], the authors analyzed various types of mechanically reconfigurable anisotropic RCCF composite patch antennas. The tuning mechanism was based on changing the current distribution on the antenna's ground plane using a unidirectional RCCF composite. Antenna tuning was achieved by mechanically rotating the RCCF ground plane in reference to the radiating elements. Square, rectangular, and slot-loaded circular patches were evaluated. The proposed method was shown to suppress resonant modes of the antenna and consequently a change in the antenna's operating frequency was observed. The isotropy of CFRP can be enhanced by adding a layer of shredded and randomly distributed carbon fibers [87]. This technique has been used to develop a ground plane for a narrowband wire monopole and an ultra-wideband conical monopole antenna. The performance of these antennas showed excellent agreement with their metallic counterparts.

CLAS Summary: Based on the examined literature relating to CLAAS and CLAS, an overview of all the different antenna topologies, frequency ranges, achieved fraction bandwidths (where possible impedance bandwidth taken ≤ -10 dB) and mechanical testing performed has been detailed in Table 4.

B. ELETRICAL, ELECTRONICS AND RF SYSTEMS

From the review of publications relating to the integration of electric and electronic systems (known here as conformal load-bearing electrical and electronics (CLEE) systems) within aircrafts smart skins, this area of CLSS is less advanced than antennas or sensors. In terms of electric systems, most of the relevant publications have focused on developing integrated electric power distribution systems. These examples have utilized airframe embedded power rails instead of traditional wire harnesses or use an aircraft body conducting

TABLE 4. Antenna Overview

Antenna Topology	*Frequency*	*Fractional Bandwidth (%)*	*Gain*	*Mechanical Testing*	*Ref No.*
Annular Slot - Reduced Surface Wave (RSW)	1.41GHz	-	10dBi	-	[36]
Balanced Antipodal Vivaldi	1.5-4GHz	90.91	5dBi	-	[36]
Bifilar Helical Dipole	1.159-1.949 GHz	50.84	-3.5 to 8dBic	-	[35]
Bistable Cylindrical Shell Antenna - Developed	0.4, 1.2 GHz	17.38, 16.67	1.8,4dBi	Snap-though, snap-back	[170]
Bistable Cylindrical Shell Antenna - Stowed	3GHz	33.33	4.1dBi	Snap-though, snap-back	[170]
Cavity Backed Slot	8.5-8.8GHz	12.64	-0.5 to 0, 1.7-3.9dBi	-	[84]
Cavity Backed Spiral	0.05-2GHz	120-174.47	0-9dBi	Flatwise Tension, Edgewise Compression, Post Impact Compression, Shear, Fatigue	[3]-[8]
Cross Slot	-	-	-	-	[3]
Dipole	0.2025-1.9GHz	1.70-50.68	2 - 5dBi	In-Plane Loading, Shear	[23], [40], [160],[161]
Dish Antenna	-	-	-	-	[159]
Disk Cone Monopole	2-10GHz	133.33	1-4dBi	-	[87]
Double Ridge WG Horn	7.5-18GHz	82.35	1-11dBi	-	[54]
Dual-band slot-loaded circular patch antenna	3.95-11.7GHz	7	1.6-6.4dBi	-	[85], [86]
Egyptian Axe Dipole	0.035-0.307GHz	1.22-8	0.05-1.9dBi	Vibration, Natural Frequency Resonance and Bending	[49]-[51], [165], [166]
Folded Monopole	0.82GHz	3.41	1.2dBi	-	[38]
Half-Loop Antenna	0.505GHz	2.18	4.8dBi	-	[37]
Helical Monopole	1.9-3.5GHz	4.12-59.25	0.54-9dBi	-	[34], [36]
Holographic/AIS	10GHz	5	12.5-14dBi	-	[33], [55], [157]
Inverted-F	0.8Ghz	-	0.14-5.07dBi	-	[32]
Log-Periodic Dipole Array	0.35-0.75GHz	72.73	6-8.5 dBi	-	[26]
L-Shaped Monopole	2.45GHz	19.9	1.4dBi	-	[20]
Meandered Dipole	0.766-3.165GHz	1.70-10.36	1.7-2.7dBi	In-Plane Loading, Shear	[25], [41], [42]
Monopole Array	2.45GHz	13.56	11dBi	-	‹21], [22]
Monopole	0.147-10GHz	14.83-66.67	-1.8 to 5.2dBi	-	[20], [80], [87], [161]
Patch	0.48-2.44GHz	1.58-6.82	-2.6-6.7dBi	Tension; Biaxial, Twisting-induced Shear Loading, Disbonding, Bending, Impact	[3], [28], [30], [31], [39], [43], [44], [52], [125], [164], [173]
Patch Array	1 - 31GHz	1.138-10	2-20.7dBi	Flatwise Tension, Bending, Impact	[12], [13], [16]-[18], [45], [52], [115], [116], [126], [137], [139]
PIFA	UHF/VHF	-	20.5dBi	-	[158]
Pixel Antenna	1.5, 2, 3.1 GHz	-	5.3dBi	Bending	[14]
Radial Slot	1.7-2.6GHz	8.33-11.11	5dBi	-	[23], [24]
Reflector Backed Dipole	3.9 GHz	13.37	6.29dBi	-	[162]
Serial Patch Array	1.79	8.92	0.5dBi	-	[46]
Slot Antenna	8.5-8.8GHz	24.14	-0.5 to 0dBi	-	[84]
Slot Coupled Patch	5.18GHz	1.72	-	Impact	[125]
Slot Log-Periodic Dipole	0.2-1.2GHz	56	>-10dBi	-	[29]
Slot Monopole	0.8Ghz	2.01	3.31dBi	-	[32]
Slotted Spiral	-	40	3.2-9dBi	Flatwise Tension and Compression	[83]
Slotted Waveguide Array	4-10GHz	1.07 - 11.16	2 - 16.67dBi	-	[71]-[78], [130], [172]
Stacked Patch	1.25-12.75 GHz	12.86-14.74	11.91-12.25dBi	Edgewise Compression and Bending	[9]-[11], [19], [163]
Stacked Patch Array	7.5 GHz	6.67	6.32dBi	-	[15]
Structural Resonator	0.163-0.8GHz	77.32	0.14-5.07dBi	-	[32], [160]
T-Shaped Monopole	2.45GHz	18.73	0.74dBi	-	[20]
Wideband Monopole	-	163.64	2-5.7dBi	-	[81], [82]
Yagi-Uda	2.08GHz	8.17	7dBi	-	[27]

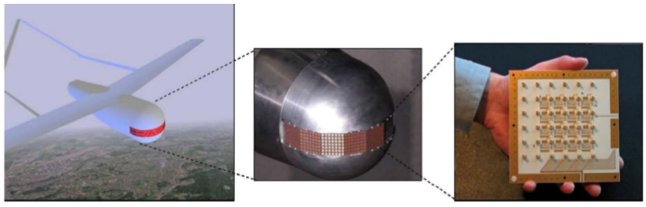

FIGURE 22. A conformal ESA system on a small UAV (left), a Ku-band conformal aperture for the nose part of an UAV (center) and a Smart Skin digital beamforming X-band antenna (right) [139].

FIGURE 23. Prototype of UAV with monocrystalline solar cells mounted in the wings as presented in [140].

element (e.g., a CFRP composite layer) as a current return network [138]. In the case of electronic systems, there have been two approaches to improve functionality. The first approach is termed board-level integration. In this approach electronic circuits are assembled using traditional PCB technologies. These integrated PCBs are then installed on the inner face or inside dedicated cavities within platforms [136]. The fundamental problem with this type of integration is maintaining stiffness and the load-bearing properties of a modified aircraft skin structure. The second approach is termed circuit-level integration. This approach focuses on higher levels of integration where electronic circuits are fabricated inside the aerospace composite structure using a more holistic design process. Circuits are built into a composite using discrete components which are connected by various conducting materials. To maintain composite integrity, the layout of this embedded PCB needs to be fabricated using novel conducting materials that do not introduce discontinuities into a laminate. They must also minimize any effects on the mechanical and load-bearing properties of a structure.

The example of a board level integration can be found in [139]. In this example the authors presented a semi-conformal, thin, and compact RF front-end GaAs MMIC agile receiver (Fig. 22). The device operated over a frequency range of 8-10 GHz and together with a digital beamforming network and an X-band antenna were installed in the nosecone of a small UAV. More examples of board-level integration can be found in [140], [141] where the functionality of UAV skins was improved by the integration of photovoltaic (PV) solar cells (known here as conformal load-bearing power generation (CLPG)). The solar cell array was designed to supplement onboard batteries to extend the platforms endurance. However, it was noted that temperature and irradiation variations did affect the performance of the PV cells and hence the UAV endurance [140]. In these reported studies it is noted that the PV cells are integrated as a CLSS [140], [141], whereas the UAV electronic systems were installed traditionally inside the airframe (Fig. 23). Flight tests showed that the wings with embedded solar cells were able to extend the platform's endurance by 15%. The integration of photovoltaic cells into UAS structures has had a long- and well-established history. Review on this technology can be form in [177], [178], [179]. There are also several successful testbed platforms (such as AeroVironment/NASA HELIOS and BAE PHASA-35).

A hybrid approach to the assembly of electronic systems which are embedded into a fixed-wing Micro Air Vehicle was reported in [142]. A part of the onboard electronics of the MAV was assembled on a flexible printed circuit membrane (FPCM) that was used to form the skin of the drone's wing. The wing skeleton was made with unidirectional carbon fiber tape. The flight parameters of the MAV were continuously measured using a micro hot-film flow speed sensor array which was distributed on the leading edge of the wing. The sensors readings were acquired by the autopilot circuit fabricated on a classic PCB which was installed within the fuselage of the MAV.

Examples of the circuit-level integration approach for CLSS applications indicate that they will have better size, weight, and power (SWaP) performance compared to the board level approach. However, from a technological point of view, the demonstrated techniques show that this level of integration is more demanding and challenging. This is because the entire circuit is encapsulated as part of the composite structure. Here, the laminate plies play the role of a substrate while also being load-bearing materials. These two requirements mean that these designs ultimately need to be carried out using multi-physics tools. This technology also requires the utilization of new conducting materials because copper foil, which is used in standard PCB manufacturing as a conductor, bonds poorly to many thermoset resins without extensive surface treatment [169]. This opens the door to explore novel conductors for this application. The introduction of new conducting materials will also require new techniques to create joints between fabricated circuit layouts and individual electronic components (resistors, capacitors, inductors, etc.). In most cases traditional PCB soldering methods may not be suitable for CLSS. Finally, with the inclusion of high-power electronic devices, new heat dissipation methods must be employed.

Silver conducting ink is one of the candidates for making the layout of smart skin embedded electronic circuits [143]. This flexible material can be printed on surfaces of many solid materials. It can also act as a substitute for soldering.

The properties of different silver inks were investigated over the RF frequency range in [143], [144]. An ink printed microstrip transmission lines, embedded into BTCy-1 6781

S-glass composite prepreg material was investigated in [143]. While silver ink was deposited on Rogers 5880 substrate in [144] to determine the conductivity of the ink over the microwave frequency range. A curve fitting method was employed to find the inks equivalent conductivity through a comparison of electromagnetic simulation and measurement results of the microstrips. A process using the embroidery of conducting threads was another technique tested for potential application in electronic aerospace smart skins. In [48] a method was described to characterize a microstrip transmission line sewn on a flexible polydimethylsiloxane substrate using an E-fiber (thin silver coated Zylon1). The conductive E-fiber was assessed for its possible application in the development of UAV smart skin electronics. The high-frequency performance of conductive threads was also studied in [145] and [146]. In these examples different sewing and stitching techniques were used to fabricate microstrip transmission lines embroidered into a pre-preg composite material. In many presented examples of CLSS antennas and composite embedded electronics, there has been the use of non-woven copper electroplated carbon-nickel veil [51], [53], [144], [147], [148], [149]. This material exhibits acceptable conductive properties at low and high-frequency ranges [148]. Both the copper-nickel–carbon veil and conductive threads have been shown to have robust mechanical properties when embedded in composite materials. In [149], the authors examined the mechanical and electromagnetic properties of microstrip lines made with veil and embroidered with conductive threads which were embedded into composite test coupons.

For the integration of active electronic components, FleX-ICs Silicon-on-Polymer technology developed by American Semiconductor provides an attractive solution for CLSS [150]. The substrates can be conformally integrated with composite structures. Flex-IC's can also be integrated using hybrid electronic concepts where existing technologies such as the carbon-nickel veil or silver inks can be used to make circuit traces while the Flex-IC's replace bulky IC packaging technologies. Within Flex-IC products portfolio, the company is currently offering flexible sensing systems, RFID, analogue-digital converters, and various types of operational amplifier circuits.

An interesting implementation of the circuit-level assembly was reported in [151]. The developed energy harvesting structure consisted of thin-film silicon solar cell and thin-film solid-state lithium-ion batteries embedded into a carbon – epoxy laminate. The tracks of the system were printed using copper nano-ink and integrated within the composite structure. The device components (including diodes and resistors) were connected to the ink traces using silver paste. The printed tracks resistance and the performance parameters of the entire system were analyzed under mechanical loading. Further studies on active electronics embedded into composite materials have resulted in a circuit-level integration of UWB Mini – Circuit ERA-4SM+ (DC - 4 GHz) ultrawideband amplifier which was investigated in [145], [146]. The circuit was developed using microstrip technology where the conductive track was constructed using an embroidered Shieldex (100/34 dtex 2ply HC) silver thread. Short copper tabs were soldered to the amplifier and associated components. These were then consolidated as part of the composite curing process on the top of the embroidered tracks to make electrical connection. The ground plane was created using an embedded copper mesh which was added in-between the lower plies of the pre-preg stack (Fig. 24).

FIGURE 24. The completed amplifier showing embroidered strapping to hold the SMD amplifier [145].

In [147] the same authors described the design of a ceramic Mini-circuits CMA-62+ wideband medium power amplifier which was embedded conformally over an air-foil shape. The substrate was made from a structural low-loss quartz fiber re-enforced polymer (QFRP) laminate encapsulated in a cyanate ester resin matrix (Lonza PT-30). The conformal amplifier bias circuit and its transmission lines were made from a non-woven copper electroplated carbon-nickel veil. Small copper foil tabs were again used as soldering points and transitions between the components and veil traces. A light-emitting diode (LED) was also embedded into the composite structure to indicate the proper level of the amplifier bias voltage. The most advanced integration of an RF circuit within an aerospace composite structure was reported in [144] and [148]. A four-way microwave switching network was embedded into a Hexply 914E S-glass prepreg laminate. This work is the first reported example of a multilayer CLSS circuit. The RF layers of the circuit were built into the composite using copper-nickel-carbon veil, while the switch control circuit was fabricated on the back of the composite structure. Conductive silver ink was also used to print some of the tracks required for the control circuitry. The circuit components were soldered directly to these printed ink pads.

In a similar approach to the design presented in [147], copper foil tabs were soldered to RF components to enlarge their contact area so that they would make electrical connection to the veil traces. The technique investigated in [144], [145], [146], [147], [148] has provided a significant advancement in the development of multifunctional conformal loadbearing structures.

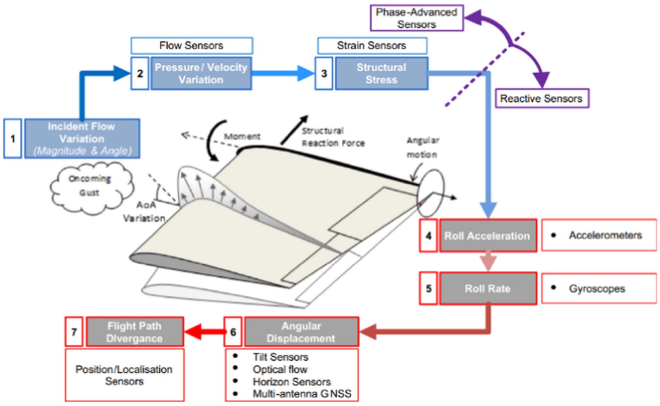

FIGURE 25. The measurable sequence of events caused by advection of turbulent properties over a wing and their attributed sensors [105].

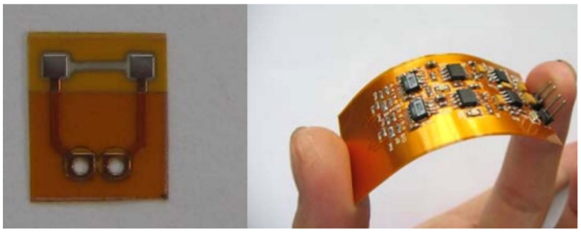

FIGURE 26. Sensors with signal conditioning circuit: a sensor unit (left); a measurement system (right) [93].

C. SENSORS

The integration of sensors into structures (known here as conformal sensors (CS)) has been the focus of structural research for several decades now. There are two major types of sensing systems designed for integration with load bearing skins of aircraft: (i) sensing systems used for structural health monitoring of the aircraft (discussed in the 'Testing and Evaluation' chapter) and (ii) sensors that minimalize human factors and allows use of automatic aircraft guidance systems. That is especially important for unmanned aerial vehicles, where sensing systems (including vision sensor systems) are responsible for controlling flight and used to create autonomous aerial machines. The sensors may be embedded in the airframe, wing, or any other part of the aircraft.

As depicted in [1], one of the highlighted areas of interest in "Project Forecast II" was the integration of small sensors systems into airframes. The fast development of UAVs, especially micro air vehicles (MAVs), and the need to control their flight parameters, has made the argument to look for smaller and more novel substitutes of traditional large sensors such as pitot tubes. Research in this area has focused on the development of distributed sensor arrays to analyze the airflow over a flying platform. The arrays were built using various types of miniature transducers (pressure sensors, hot-film resistive sensors or artificial hair sensors) integrated within UAV bodies [88]. The measured flow data was used to determine aerodynamic parameters such as angle of attack, sideslip angle, flow separation, stall, and airspeed.

Various sensing systems can combat wind gusts and violent perturbation allowing a UAV to complete a mission [106]. Fig. 25 illustrates different sensing approaches to measure and counteract the phenomena that affect the aircraft [105].

Hot-film Sensors: The hot-film flow anemometer is a sensor that converts fluctuating airflow conditions into a measurable resistance. The temperature of the sensing resistor is maintained above the airflow's ambient temperature through ohmic heating. As air passes over the sensor a temperature change is induced due to convective heat transfer. This changes the resistance of the sensing element and therefore its ability to pass current. A conditioning circuit is then used to convert the sensed current into a corresponding voltage. There are two main types of hot-film anemometers that have been reported in literature. These are based on constant current or constant temperature. The drawback of these two types of sensors includes their high sensitivity to ambient conditions and susceptibility to electromagnetic interference. Except for some limited flight applications, they had been mainly used for laboratory measurements due to the need for controlled environmental conditions [89]. In the early '90s constant voltage anemometers were introduced which were found to be immune to operational conditions, electromagnetic interference and had a higher signal to noise ratio.

In reported investigations, commercially available sensors [90], [91] and custom hot-film sensors were developed for sensing airflow using CLSS concepts [89], [92], [93], [94], [95]. Customized sensors were manufactured on flexible and low thermal conductive substrates. These sensors were then conformally integrated on to airframe surfaces. These more advanced sensors were developed using thin-film deposition methods which were applied to fabricate both the thermal element and its terminals.

Hot-film sensors have been installed on surfaces of wings of various aircraft including the F-15B flight test fixture [89], [90], and different types of MAV's [91], [92], [93], [94], [95]. Sample of hot-film sensing system is illustrated in Fig. 26.

Their performance was experimentally verified in wind tunnel tests as well as in limited flight trials. To accurately ascertain airflow conditions complex signal processing techniques, including a back-propagation neural network [91], [94] were used to extract aerodynamic and flight parameters such as airspeed, angle of attack, angle of sideslip, stall detection, flutter, and catastrophic unsteady loads [89].

Pressure Sensors: Pressure sensors can also be integrated within aircraft skins to monitor aerodynamic flight conditions. Two types of pressure transducers have been explored for CLSS applications within literature. The first is a capacitive type of sensor [96], [97], [98], [99], [100], [101] built using two sheet electrodes separated by a dielectric layer. This is usually provided by an air gap that's forms a parallel plate capacitor. One of the sensor's electrodes is formed on a membrane which can be displaced with changes in pressure. As

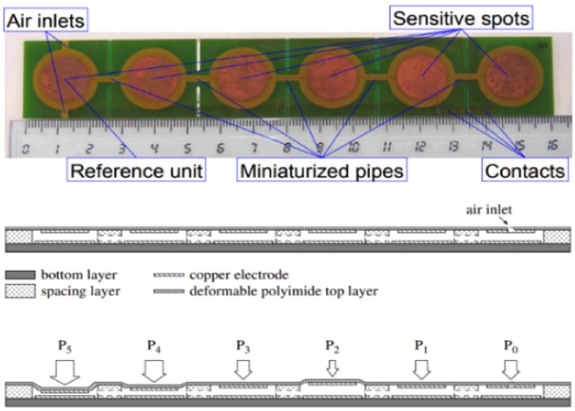

FIGURE 27. Prototype sensor array in PCB technology used in the experiments (top); sections relaxed – ambient pressure (middle); Deformed by pressure values P1 to P6 (bottom) as presented in [99].

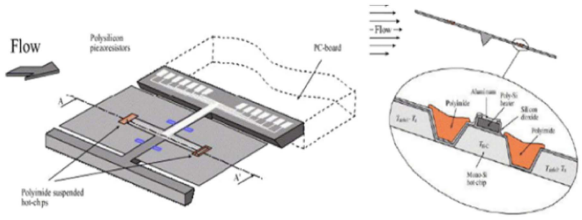

FIGURE 28. Lift force flow sensor (left) schematic of the flat plate sensing element (right) – presented in [105].

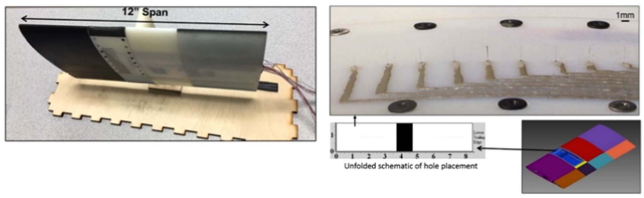

FIGURE 29. 3-D printed NACA2410 wing with a hair integrated sensors (left); Enlarged picture of the removable skin section with hair sensors and silver traces [106].

the membrane changes its distance, the sensor changes its capacitance [96]. The concept is illustrated in Fig. 27.

A signal conditioning circuit then converts these changes into a corresponding voltage or current variation. The second type of pressure transducer explored is made using micro-electromechanical system (MEMS) technology [102], [103], [104]. These devices use a diaphragm with a secured piezo-resistor element connected to form part of a Wheatstone bridge circuit. Changes in pressure deform the diaphragm which changes the piezo-resistors resistance. This results in an unbalancing of the bridge. The bridge output voltage can then be used to calculate the applied pressure.

In reported experiments, an array of capacitive pressure transducers had been integrated on the surface of a wing. However, piezo-resistive sensors were embedded inside a structure where small holes were drilled to sense the air pressure. Capacitive sensors were tested in wind tunnels and in-flight and have been installed on air foils (NACA 0012 [96]; NACA 0015 [99], [100]; NACA 2412 [101]) and various types of UAVs. Some examples include new UAV designs [102] and commercially available platforms such as the Bixler-2 [103] and Skywalker X8 Flying Wing [104].

MEMS transducers typically have low accuracy and have been operated in distributed sensor networks to significantly reduce measurement error [98], [104]. Using pressure gradients on an aircraft surface has allowed the determination of air speed, angle of attack and sideslip angle [104]. More complex signal processing methods such as machine learning algorithms based on artificial neural networks and linear regressions were employed to process the sensor signals and evaluate these flight parameters.

Biologically Inspired Sensors: High intensity turbulence at low flight levels in the Atmospheric Boundary Layer (ABL) has been shown to significantly affect flight stability of small UAVs and MAVs [105]. These types of smaller platforms require flight control systems which are equipped with fast-response sensors to measure dynamically varying aerodynamic conditions. Recent investigations into biologically inspired sensors have shown promise as an alternative for conventional transducers due to their high inertia response.

Biologically inspired sensors have been designed to imitate the reaction of mechanoreceptors of insects (i.e., hairs) or birds (i.e., feathers) when interacting with the airflow. A few types of sensors have been proposed [105] and illustrated in Fig. 28. These include MEMS transducers that operate on changes in a device's capacitance or resistance.

For example, the experimental performance of an artificial array of hair sensors (AHSs) partially embedded in a NACA2410 air foil was described in [106] and illustrated in Fig. 29. These sensing elements were built around a glass fiber (8 μm diameter) partially covered by a radially grown carbon nanotube (CNT) forest. The CNT was loosely located between two surrounding electrodes creating a resistive element. On interaction with the surrounding airflow, the deflected sensor changed its contact resistance with the electrode. A feed-forward neural network was used to process sensors signals which were used to predict aerodynamic parameters such as lift, moment coefficients, angle of attack, and freestream velocity.

Structural Health Monitoring Using Radio Frequency and Microwave Methods: RF and microwave non-destructive testing techniques have also been considered as a potential candidate for aerospace smart skin structural monitoring. The principal operation for this group of sensors is based on detecting and analyzing changes to the resonant response of one or more electrically conducting elements which have been integrated within an aircraft structure. The sensors are then excited by an external electromagnetic source such as an antenna. The sensing elements are designed in the way that their resonant frequency is strongly dependent on the instantaneous

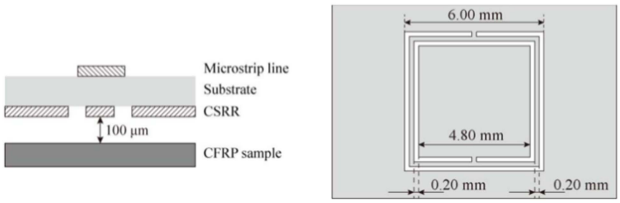

FIGURE 30. Setup (left) and geometry (right) of complementary split-ring resonator (CSRR) used for impact detection as presented in [118].

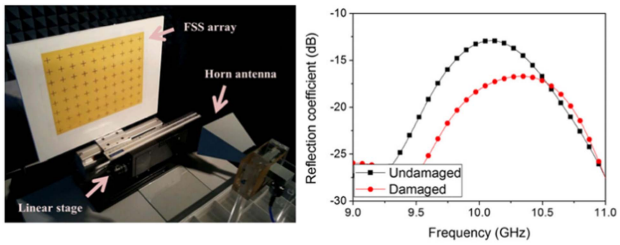

FIGURE 31. Experimental setup for structural damage localization test (left); Test result of damage effect on FSS array (right) as presented in [122].

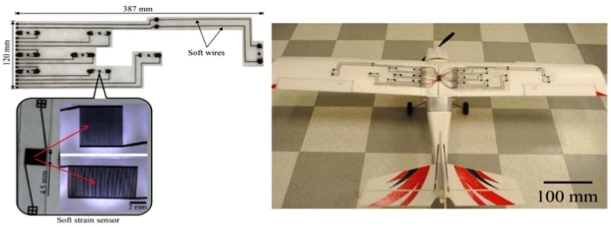

FIGURE 32. The cPDMS strain sensors (left) ; sensor array setup on the wing (right); [124].

mechanical condition required to monitor a structure. Not only can sensors be added to a structure, but large components or the entire aircraft structure can be turned into a sensor using the principals of self-resonant frequencies [32]. This type of structural health monitoring (SHM) was proposed in [117], [118], [119] to develop a wireless RF SHM method (Illustrated in Fig. 30).

The UAV's CFRP wings and rotor blades were considered as dipole antennas. It was demonstrated that the resonant response of these novel radiators, as well as their matching conditions (return losses), can be used to detect and localize wing or blade damage.

In [120], the strain analysis of an aluminum plate integrated with a 1.5 GHz microstrip circular patch antenna was presented. A theoretically derived linear relationship between the shift of an antenna's resonant frequency and its applied strain was confirmed experimentally and numerically using mechanical and electromagnetic co-simulation (ANSYS). This work followed by the investigation of this type of antenna on a square CFRP panel. [121]. It was noted that the drawback of this type of sensor was its directional properties which manifested from its low sensitivity to strain caused by diagonal bending in a composite panel. This problem was addressed by changing the frequency to 3.5 GHz and the antenna to a meandered circular microstrip patch. The new sensor had omnidirectional strain sensing ability and had three times higher sensitivity while being five times smaller.

Another possible microwave SHM method was reported in [122] where a frequency selective surface (FSS) was proposed for wireless monitoring of strain and damage of glass-reinforced epoxy composites structures. The multi-element FSS was designed to operate at a frequency of 10 GHz and was fabricated on a flexible polyimide printed circuit board (PCB) membrane. This was then embedded into the host material to enable sensing of the structure. A horn antenna was used to measure the frequency response of the FSS, specifically its reflection coefficient. The damage to individual FSS elements in this example caused local inhomogeneity in the surface's response. These changes were able to be detected and help localize any areas which were damaged. Validation of this sensor is shown in Fig. 31.

Other SHM method: There have also been other smart skin structural monitoring techniques investigated. The strain and damage monitoring of CFRP through DC resistance measured by a multi-electrode test system was discussed in [123]. The test electrodes were fabricated on flexible PCB substrates and integrated within carbon fiber composite panels. The system exhibited high measurement accuracy when compared with ultrasonic C-scanning methods.

The proposed method was able to detect, locate, and assess damage severity effectively on both the surface and through-thickness of CFRP panels. UAV wind deflection and strain, monitored by an array of eight soft-strain interdigital capacitive sensors, were described in [124]. The sensors and their electrical wires were fabricated on a flexible and stretchable polydimethylsiloxane (PDMS) substrate using conductive polydimethylsiloxane (cPDMS). The PDMS substrate was then bonded onto a UAV wing using a silicone adhesive. A static laboratory wing test was carried out and a linear relationship between the sensors capacitance and wing loading was reported. The sensor design and the layout of the sensors is illustrated in Fig. 32.

D. THERMAL MANAGEMENT

Electronic systems and wiring harnesses integrated within an aircraft body generate heat. Temperature control is critical for many of these systems to operate flawlessly and safely. Outlined in [1], thermal management figure shown here as conformal load-bearing thermal management (CLTM)) will also play a critical role in the design of aerospace smart skins. Unfortunately, this area has not been explored as extensively as other areas of CLSS. The primary reason for this is likely due to the small body of research related to the integration of active electronics embedded in structures. As a result, the has not been an identified problem with heat management nor has there been a need to examine different heat dissipation methods. The most advanced research carried out on

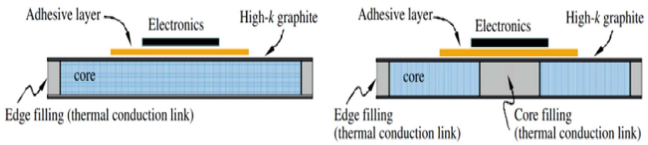

FIGURE 33. The thermal control with high thermal conductive fiber and thermal link: (left) edge filling and (right) core filling as presented in [136].

heat management problems was related to designs of multifunctional structures for space applications [134]. In contrast, reported studies about corresponding constructions used in aircraft and UAVs are few and far between.

Presented in [135] was a method of bonding an electronic circuit board to an aluminum honeycomb space structure. The multichip module (MCM) heat rejection and thermal control efficiency were assessed for various cooling system configurations. The most efficient setup consisted of a MCM which incorporated an isotropic carbon-carbon thermal doubler between the MCM and Honeycomb structure. The MCM was secured to the honeycomb structure with high thermal conductivity (Hi-K) composite face sheets filler. It was found that the thermal doubler reduced the overall thermal gradient between the MCM ceramic low temperature co-fired alumina base and the temperature-controlled aluminum honeycomb space structure. As mentioned, this configuration exhibited the best performance and was capable of dissipating around 14W/cm2 of energy.

Another proposed solution to thermal management in space structures was studied in [136]. The concept of thermal management is illustrated in Fig. 33. The onboard electronic PCBs were embedded into the spacecraft panel and were in direct contact with the spacecraft's outer radiative skin through a thin layer shielding case. The shielding case maintained structural stiffness and protected the electronics against radiation while providing a reasonable heat transfer media. The cooling mechanism was based on a thermal conduction at the interface between the electronics and the radiative skin. Heat was dissipated by radiation from the radiative skin and 3 degrees kelvin space. Laboratory tests of the fabricated smart skin with embedded electronics showed efficient performance of the cooling system. The structure was also found to have a few other benefits such as being 40% lighter and reducing it utilized volume by 90% when compared to a traditional configuration.

In [13] the authors reported a passive cooling system for electronics embedded into a sandwich structure. This consisted of a carbon/epoxy sheets which were separated with a polyurethane foam core. This structure was investigated for UAV applications. The proposed system included the use of heat pipes and a thermal interface material (TIM) to distribute heat. The heat pipe thermal management system was based on the capillary action phenomenon. The TIM comprised of a copper silicone elastomer composite. During the cooling process, heat was rejected from electronics through the TIM. The heat energy was then transferred into the UAV skin using heat pipes where it was dissipated by convective cooling from air passing over the outer skin.

An alternative method of thermal management of avionic electronics systems was presented in [137]. The authors presented a highly integrated design of an aircraft active skin antenna which included an embedded microchannel cooling system. The structure consisted of a 64 element microstrip patch phased array antenna that was integrated with transceiver chips and feeding network. The structure was fabricated into a multilayer Ferro A6-S low temperature co-fired ceramic (LTCC) structure. A microchannel heat sink was also fabricated into the LTCC process and integrated into various substrate layers. Because of the low heat transfer coefficient of LTCC, copper cylinders were used to improve the efficiency of heat transfer between transmitter chips and microchannel coolant. The geometry of the channels was optimized to achieve uniform heat distribution across the heat sink structure and to ensure efficient cooling all of the transceiver elements.

V. KEY CHALLENGES AND FUTURE PROSPECTS

A. FUTURE DIRECTION OF CLSS AND KEY AREAS THAT NEED EXPLORING

The CLSS concept provides an opportunity to combine communication and navigation systems into one multiband composite structure which is integrated seamlessly into the external geometry of an aircraft or UAV. Integration of radiating elements and electronics into the load bearing skin, as well as achieving resistance to impact or damage is still a challenge for CLSS. Integration of traditional 'black box' polymer or ceramic IC/MMIC packed devices also significantly limits the level of integration for CLSS. Based on the review of the literature on CLSS, the future direction is to further maximize the integration of RF elements and electronics into aircraft skins to the level of complete assimilation. Further exploration and development of new materials which are lighter, stronger mechanically and at the same time able to mechanically self-repair and correct their electrical and electromagnetic responses is necessary to further this area.

The key fields that need to be explored for further development of CLSS are as follows:

- New materials which are lighter and stronger as load bearing structures.
- Self-repairing composite structures capable of withstanding high velocity impacts.
- Liquid low-resistance conductors that can be used in self-repair and compensation of RF circuitry.
- Flexible electronic and RF systems including 3D printed circuits and lumped elements.
- Manufacturing technologies and processes to totally integrate micro-electronic components and electromagnetic structures with load bearing skins and

doing so without causing loss to the skin's structural properties.
- Further use of MEMS, IC, MMIC with CLSS.
- Find techniques to repair CLSS structures
- Understanding of how mechanical loads effect the reliability of connectors (DC-RF) used to feed CLSS.

B. FUTURE MANUFACTURING TECHNIQUES NEEDED FOR ADVANCING CLSS

Future manufacturing techniques follow the current trends in manufacturing at large. This includes steps to automate assembly, prevent failures, optimize the manufacturing process, and minimize costs. The following trends are mentioned:

- 3D printing is cost-effective, efficient, and scalable, and which results in the use of fewer materials and the creation of less waste compared to more traditional manufacturing methods.
- Multi-material additive technology such as the nScript or Flex-IC technology for use in the manufacture of components and assemblies.
- Use of artificial intelligence (AI) as a generative design tool for CLSS and to also identify/detect failure patterns in CLSS aircraft components.
- Use of 'digital twins' to simulate new products and assess how they might operate under certain real-world conditions.
- Advanced automation accommodates more manufacturing tasks. This is achieved through extended use of robotic assembly.

C. STATES ON REFERENCES

One hundred and seventy-six research papers were reviewed to evaluate the current state of CLSS technology. They refer to a variety of interconnected fields such as: antenna and other RF components, sensors and sensing platforms, electrical and testing systems. Based on research to date, there are opportunities to expand research into:

- Antenna and other RF components:
  - Further research into multiband phased antenna as an integral part of the skin with no loss of structural properties.
  - Further development of self-correcting and adjusting antenna in response to surrounding elements like stress, temperature etc.
  - Development of flexible antenna structures based on liquid conductors.
- Structural monitoring sensors and environmental change sensors:
  - Further design and development of MEMS technology directed towards structural monitoring and self-repairing and environmental sensing.
  - Achieving total integration of intelligent sensing systems with CLSS to the point where a sensing system becomes a load bearing skin.
  - Development of self-healing technology to reduce structural damage of CLSS caused by the external impacts.
- Electronic systems:
  - Development of a sensing microsystems network interconnected throughout the skin to protect CLSS stability and allow total control of UAV behavior.
  - Further development of flexible polymer-based substrates and technology that allow insertion and connection of semiconductor dies directly to those substrates.
  - Further research on conductive polymers with a view to utilizing them in UAVs.

VI. CONCLUSION

This review has provided an overview of all the literature that is related to the design and evaluation of different CLSS concepts. Since the initial inception of CLSS was proposed in the 1990's, it has been shown that this field of research has continued to expand over the past three decades. It has also highlighted the raft of different applications and technologies explored for this application. However, it is also clear that there is still a significant amount of investigation that is required to see the wider adoption of this technology. The large focus areas of antennas and sensors have provided significant developments which can provide tangible SWaP benefits. However, it is also clear that these fields are only the tip of what CLSS can potentially achieve. For example, the integration of complete systems within composite structures is one area where there is a clear need for future developments. There are several technologies which a are now making this area more viable such as the introduction of multi-material additive manufacturing technologies (such as the nScrypt) and American Semiconductor's Flex-IC packaging technology.

The review of literature indicated that CLSS are, predominantly, separately built multilayer structures which are embedded into parts of an aircraft skin or frame. The level of integration between CLSS and surrounding support (skin or frame) depends on the CLSS's size and its structural complexity. Persistent issues with bonding dissimilar materials remain the biggest hurdle to the widespread adoption of current CLSS. Future iterations of CLSS will need to overcome this piece-wise integration and adopt a more holistic manufacturing approach.

A variety of CLSS examples discussed in this review provided multiple technological solutions and at the same time described the difficulties that may affect the performance of their parent structure. One overarching conclusion that has come out of this review is that future research should be concentrated on the development of materials, technologies and manufacturing processes that would allow CLSS, containing a variety of microwave and sensing systems with purposefully dedicated electronics, to be fully integrated with the surrounding skin of an aircraft and governed by an embedded artificial intelligence system. The resulting outcome would enable CLSS to become a holistic system within the skin or frame of any aerospace platform.

REFERENCES

[1] T. L. Thomas, "Development of robust hybrids for smart skin avionics," in *Proc. IEEE 40th Conf. Proc. Electron. Compon. Technol.*, 1990, pp. 131–139.

[2] J. W. Cananu, "SAF in the twenty-first century," *Air Force Mag.*, vol. 9, pp. 47–52, Aug. 1986.

[3] M. Hopkins, J. Tuss, A. Lockyer, K. Alt, R. Kinslow, and J. Kudva, "Smart skin conformal load-bearing antenna and other smart structures developments," in *Proc. 38th Struct., Struct. Dyn., Mater. Conf.*, 1997, pp. 521–530.

[4] A. J. Lockyer, K. Kinslow, R. Kan, and K. J. Han-Pin, "Development of a structurally integrated conformal load-bearing multifunction antenna: Overview of the air force smart skin structures technology demonstration program," *Proc. SPIE*, vol. 2722, pp. 55–64, May 1996.

[5] A. J. Lockyer, K. H. Alt, J. N. Kudva, R. W. Kinslow, and A. C. Goetz, "Conformal load-bearing antenna structures (CLAS): Initiative for multiple military and commercial applications," *Proc. SPIE*, vol. 3046, pp. 182–196, Jun. 1997.

[6] A. J. Lockyer, K. H. Alt, D. P. Coughlin, M. D. Durham, and J. N. Kudva, "Design and development of a conformal loadbearing smart skin antenna: Overview of the AFRL smart skin structures technology demonstration (S3TD)," *Proc. SPIE*, vol. 3674, pp. 410–424, Jul. 1999.

[7] A. J. Lockyer, K. H. Alt, and J. N. Kudva, "Air vehicle integration issues and considerations for CLAS successful implementation," *Proc. SPIE*, vol. 4332, pp. 48–59, Jun. 2001.

[8] D. Kim, J. Kim, J. Kim, and M. Kim, "Design and fabrication of a composite antenna-structure for broadband frequency with microwave absorber," *J. Composite Mater.*, vol. 46, no. 15, pp. 1851–1858, Jul. 2012.

[9] C. S. You and W. Hwang, "Design of load-bearing antenna structures by embedding technology of microstrip antenna in composite sandwich structure," *Composite Structures*, vol. 71, no. 3/4, pp. 378–382, 2005.

[10] C. S. You and W. Hwang, "Design and fabrication of composite smart structures with high electrical and mechanical performances for future mobile communication," *Mechanics Composite Mater.*, vol. 40, no. 3, pp. 237–246, 2004.

[11] C. S. You, W. Hwang, and S. Y. Eom, "Design and fabrication of composite smart structures for communication, using structural resonance of radiated field," *Smart Mater. Structures*, vol. 14, no. 2, pp. 441–448, 2005.

[12] P. Li, W. Y. Xu, L. W. Song, and Y. Y. Qiu, "A novel inversion method of manufacturing flaws in the packaging of conformal loadbearing antenna structure," *Int. J. Antennas Propag.*, vol. 2015, pp. 1–13, Sep. 2015.

[13] J. Zhou, J. Huang, L. Song, D. Zhang, and Y. Ma, "Electromechanical co-design and experiment of structurally integrated antenna," *Smart Mater. Structures*, vol. 24, no. 3, 2015, Art. no. 037004.

[14] M. Ali, N. Bishop, W. Baron, B. Smyers, J. Tuss, and D. Zeppettella, "A MEMS reconfigurable pixel microstrip patch antenna for conformal load bearing antenna structures (CLAS) concept," in *Proc. IEEE Antennas Propag. Soc. Int. Symp.*, 2014, pp. 1093–1094.

[15] S. H. Son, S. Y. Eom, and W. Hwang, "Development of a smart-skin phased array system with a honeycomb sandwich microstrip antenna," *Smart Mater. Structures*, vol. 17, no. 3, Jun. 2008, Art. no. 035012.

[16] S. Dweik, S. Deif, W. Sadeh, O. A. Rawashdeh, D. N. Aloi, and M. S. Sharawi, "A planar antenna array with integrated feed network for UAV applications," in *Proc. 8th Eur. Conf. Antennas Propag.*, 2014, pp. 1855–1858.

[17] M. Ibrahim, S. Deif, and M. S. Sharawi, "A 14-element printed planar array embedded within a UAV structure," in *Proc. Loughborough Antennas Propag. Conf.*, 2012, pp. 1–4.

[18] M. S. Sharawi, M. Ibrahim, S. Dief, and D. N. Aloi, "Planar printed antenna array embedded in the wing structure of a UAV for communication link enhancement," *Prog. Electromagn. Res.*, vol. 138, pp. 697–715, 2013.

[19] E. T. Rahardjo, F. Y. Zulkifli, Basari, D. Y. H. Basari, and J. T. Sri Sumantyo, "Circularly polarized microstrip antenna array for UAV application," in *Proc. Int. Symp. Antennas Propag.*, 2013, pp. 870–872.

[20] M. S. Sharawi, O. A. Rawashdeh, and D. N. Aloi, "2.4 GHz printed antennas embedded in small UAV wing structures," *J. Electromagn. Waves Appl.*, vol. 24, pp. 463–474, 2010.

[21] M. S. Sharawi, D. N. Aloi, and O. A. Rawashdeh, "Design and implementation of embedded printed antenna arrays in small UAV wing structures," *IEEE Trans. Antennas Propag.*, vol. 58, no. 8, pp. 2531–2538, Aug. 2010.

[22] M. S. Sharawi, O. A. Rwashdeh, and D. N. Aloi, "Performance of an embedded monopole antenna array in a UAV wing structure," in *Proc. IEEE 15th Mediterranean Electrotech. Conf.*, 2010, pp. 835–838.

[23] D. M. Moorehouse and A. Humen, "Improved UAV datalink performance using embedded antennas," Nurad Technologies, Baltimore, MD, USA, Tech. Rep. 21215, 2023.

[24] A. Patrovsky and R. Sekora, "Structural integration of a thin conformal annular slot antenna for UAV applications," in *Proc. Antennas Propag. Conf.*, 2010, pp. 229–232.

[25] S. - M. Yang and C. - H. Huang, "An inductor model for analyzing the performance of printed meander line antennas is smart structures," *J. Electromagn. Anal. Appl.*, vol. 6, pp. 244–252, 2014.

[26] N. A. Bishop, J. Miller, D. Zeppettella, W. Baron, J. Tuss, and M. Ali, "A broadband high-gain bi-layer LPDA for UHF conformal loadbearing antenna structures (CLASs) applications," *IEEE Trans. Antennas Propag.*, vol. 63, no. 5, pp. 2359–2364, May 2015.

[27] M. Wright, M. Ali, W. Baron, J. Miller, J. Tuss, and D. Zeppettella, "Conformal direct written antenna on structural composites," in *Proc. IEEE Int. Symp. Antennas Propag. USNC/URSI Nat. Radio Sci. Meeting*, 2015, pp. 613–614.

[28] G. S. Karthikeya, N. Agnihotri, S. S. Siddiq, K. S. Mehul, and T. Thyagaraj, "A conformal UHF antenna for cargo helicopter belly," in *Proc. IEEE 5th Asia-Pacific Conf. Antennas Propag.*, 2016, pp. 285–286.

[29] M. Kim, C. Park, C. Cho, and S. Jun, "A multi-band smart skin antenna design for flight demonstration," in *Proc. 8th Eur. Conf. Antennas Propag.*, 2014, pp. 2855–2859.

[30] C. Chen and H. Zheng, "Design of a dual-band conformal antenna on a cone surface for missile-borne," in *Proc. IEEE 5th Asia-Pacific Conf. Antennas Propag.*, 2017, pp. 1–3.

[31] J. Wu, J. Yu, and Q. Tao, "Design of a missile-borne conformal microstrip navigation antenna," in *Proc. EITCE, MATEC Web Conferences*, 2018, pp. 1–5.

[32] Y. Chen and C.-F. Wang, "HF band shipboard antenna design using characteristic modes," *IEEE Trans. Antennas Propag.*, vol. 63, no. 3, pp. 1004–1013, Mar. 2015.

[33] K. J. Nicholson, T. C. Baum, J. E. Patniotis, and K. Ghorbani, "Discrete holographic antenna embedded in a structural composite laminate," *IEEE Antennas Wireless Propag. Lett.*, vol. 19, no. 2, pp. 358–362, Feb. 2020.

[34] N. Neveu et al., "Miniature hexaferrite axial-mode helical antenna for unmanned aerial vehicle applications," *IEEE Trans. Magn.*, vol. 49, no. 7, pp. 4265–4268, Jul. 2013.

[35] B. T. Stojny and R. G. Rojas, "Bifilar helix GNSS antenna for unmanned aerial vehicle applications," *IEEE Antennas Wireless Propag. Lett.*, vol. 13, pp. 1164–1167, 2014.

[36] R. L. Cravey, E. Vedeler, L. Goins, W. R. Young, and R. W. Lawrence, "Structurally integrated antenna concepts for HALE UAVs," NASA Langley Res. Cntr., Hampton, VA, USA, Tech. Rep. NASA/TM-2006-214513, 2006.

[37] B. - H. Sun, Y. - F. Wei, S. - G. Zhou, and Q. - Z. Liu, "Low-profile and horizontally-polarised antenna for UAV applications," *Electron. Lett.*, vol. 45, no. 22, 2009, pp. 1106–1107.

[38] Z. Liu, Y. Zhang, Z. Qian, Z. P. Han, and W. Ni, "A novel broad beamwidth conformal antenna on unmanned aerial vehicle," *IEEE Antennas Wireless Propag. Lett.*, vol. 11, pp. 196–199, 2012.

[39] Y. Zhou, Y. Bayram, L. Dai, and J. L. Volakis, "Conformal loadbearing polymer-carbon nanotube antennas and RF front-ends," in *Proc. IEEE Antennas Propag. Soc. Int. Symp.*, 2009, pp. 1–4.

[40] D. J. Hartl, G. J. Frank, G. H. Huff, and J. W. Baur, "A liquid metal-based structurally embedded vascular antenna: I. Concept and multiphysical modeling," *Smart Mater. Structures*, vol. 26, no. 2, 2017, Art. no. 025001.

[41] D. J. Hartl, G. J. Frank, R. J. Malak, and J. W. Baur, "A liquid metal-based structurally embedded vascular antenna: II. Multiobjective and parameterized design exploration," *Smart Mater. Structures*, vol. 26, no. 2, 2017, Art. no. 025002.

[42] G. H. Huff, H. Pan, D. J. Hartl, G. J. Frank, R. L. Bradford, and J. W. Baur, "A physically reconfigurable structurally embedded vascular antenna," *IEEE Trans. Antennas Propag.*, vol. 65, no. 5, pp. 2282–2288, May 2017.

[43] Y. Bayram et al., "E-textile conductors and polymer composites for conformal lightweight antennas," *IEEE Trans. Antennas Propag.*, vol. 58, no. 8, pp. 2730–2736, Aug. 2010.

[44] F. Xu, B. Wei, W. Li, J. Liu, W. Liu, and Y. Qiu, "Cylindrical conformal single-patch microstrip antennas based on three dimensional woven glass fibre/epoxy resin composites," *Composites B*, vol. 78, pp. 331–337, 2015.

[45] F. Xu and Y. Qiu, "Simulation and electromagnetic performance of cylindrical two-element microstrip antenna array integrated in 3D woven glass fibre/epoxy composites," *Mater. Des.*, vol. 89, pp. 1048–1056, 2016.

[46] C. -Z. Du, S. -S. Zhong, L. Yao, and Y.-P. Qiu, "Textile microstrip array antenna on three-dimensional orthogonal woven composite," in *Proc. 4th Eur. Conf. Antennas Propag.*, 2010, pp. 1–2.

[47] Z. Wang, L. Zhang, Y. Bayram, and J. L. Volakis, "Embroidered e-fibre polymer composites for conformal and load bearing antennas," in *Proc. IEEE Antennas Propag. Soc. Int. Symp.*, 2010, pp. 1–4.

[48] Z. Wang, L. Zhang, Y. Bayram, and J. L. Volakis, "Multilayer printing of embroidered RF circuits on polymer composites," in *Proc. IEEE Antennas Propag. Soc. Int. Symp.*, 2011, pp. 278–281.

[49] K. J. Nicholson, T. C. Baum, K. Ghorbani, and R. W. Ziolkowski, "Metamaterial-inspired electrically small antennas integrated into structural materials," in *Proc. Int. Symp. Antennas Propag.*, 2015, pp. 1–4.

[50] T. C. Baum, K. Ghorbani, A. Galehdar, K. J. Nicholson, and R. W. Ziolkowski, "Multi-functional composite metamaterial-inspired EEAD antenna for structural applications," in *Proc. Int. Workshop Antenna Technol.*, 2016, pp. 144–147.

[51] T. C. Baum, R. W. Ziolkowski, K. Ghorbani, and K. J. Nicholson, "Investigations of a load-bearing composite electrically small Egyptian axe dipole antenna," *IEEE Trans. Antennas Propag.*, vol. 65, no. 8, pp. 3827–3837, Aug. 2017.

[52] K. Alagiyawanna, T. C. Baum, K. Ghorbani, and K. J. Nicholson, "Embroidered microwave antennas for aerospace applications," in *Proc. Asia-Pacific Microw. Conf.*, 2016, pp. 1–4.

[53] T. C. Baum, K. J. Nicholson, K. Ghorbani, and R. W. Ziolkowski, "Passive and active metamaterial-inspired radiating and scattering systems integrated into structural composite materials," in *Proc. IEEE 11th Int. Congr. Engineered Mater. Platforms Novel Wave Phenomena*, 2017, pp. 400–402.

[54] K. V. Hoel, S. Kristoffersen, J. Moen, G. Holm, and T. S. Lande, "Characterization of a 3D printed wideband waveguide and horn antenna structure embedded in a UAV wing," in *Proc. IEEE 10th Eur. Conf. Antennas Propag.*, 2016, pp. 1–4.

[55] E. Gupta, C. Bonner, N. Lazarus, M. S. Mirotznik, and K. J. Nicholson, "Multi-axis manufacture of conformal metasurface antennas," *IEEE Antennas Wireless Propag. Lett.*, vol. 22, no. 11, pp. 2629–2633, Nov. 2023.

[56] C. L. Holloway, M. S. Sarto, and M. Johansson, "Analysing carbon-fibre composite materials with equivalent-layer models," *IEEE Trans. Electromagn. Compat.*, vol. 47, no. 4, pp. 833–844, Nov. 2005.

[57] T. Doan, A. Walters, and C. Leat, "Characterisation of electromagnetic properties of carbon fibre composite materials," in *Proc. Electromagn. Compat. Symp.*, 2009, pp. 87–91.

[58] A. Galehdar, K. Nicholson, K. S. T. Rowe, and K. Ghorbani, "The conductivity of unidirectional and quasi isotropic carbon fibre composites," in *Proc. 40th Eur. Microw. Conf.*, 2010, pp. 882–885.

[59] A. Galehdar, W. S. T. Rowe, and K. Ghorbani, "The effect of ply orientation on the performance of antennas in or on carbon fibre composites," *Prog. Electromagn. Res.*, vol. 116, pp. 123–136, 2011.

[60] M. Rudd, T. C. Baum, K. J. Nicholson, and K. Ghorbani, "Estimating the conductivity of carbon fibre veil (CFV) based on shielding effectiveness," in *Proc. IEEE Asia Pacific Microw. Conf.*, 2017, pp. 1034–1036.

[61] M. Rudd, T. C. Baum, and K. Ghorbani, "Determining high-frequency conductivity based on shielding effectiveness measurement using rectangular waveguides," *IEEE Trans. Instrum. Meas.*, vol. 69, no. 1, pp. 155–162, Jan. 2020.

[62] A. Bojovschi, K. J. Nicholson, A. Galehdar, P. J. Callus, and K. Ghorbani, "The role of fibre orientation on the electromagnetic performance of waveguides manufactured from carbon fibre reinforced plastic," *Prog. Electromagn. Res. B*, vol. 39, pp. 267–280, Mar. 2012.

[63] E. J. Riley, E. H. Lenzing, and R. M. Narayanan, "Characterization of carbon fibre composite materials for RF applications," *Proc. SPIE*, vol. 814, May 2014, Art. no. 9077.

[64] S. Gona, P. Tomasek, and V. Kresalek, "Measurement of conductivity of carbon fibres at microwave frequencies," in *Proc. 23rd Int. Conf. Radioelektronika*, 2013, pp. 68–71.

[65] A. Galehdar, P. J. Callus, and K. Ghorbani, "A novel method of conductivity measurements for carbon-fibre monopole antenna," *IEEE Trans. Antennas Propag.*, vol. 59, no. 6, pp. 2120–2126, Jun. 2011.

[66] M. Rudd, T. C. Baum, B. Mapleback, K. Ghorbani, and K. J. Nicholson, "Reducing the attenuation in CFRP waveguide using carbon fibre veil," *IEEE Microw. Wireless Compon. Lett.*, vol. 27, no. 12, pp. 1089–1091, Nov. 2017.

[67] R. Wagner, "Carbon fibre slotted waveguide arrays," in *Proc. Mil. Microw. Conf*, 1986, pp. 231–236.

[68] P. J. Callus, "Conformal load bearing antenna structure for Australian Defence Force aircraf," Defense Tech. Inf. Cntr., Fort Belvoir, VA, USA, Tech. Rep. DSTO-TR-1963, 2007.

[69] P. J. Callus, "Novel concepts for conformal load-bearing antenna structure," Defense Tech. Inf. Cntr., Fort Belvoir, VA, USA, Tech. Rep. DSTO-TR-2096, 2008.

[70] D. Gray, K. J. Nicholson, K. Ghorbani, and P. J. Callus, "Carbon fibre reinforced plastic slotted waveguide antenna," in *Proc. Asia–Pacific Microw. Conf.*, 2010, pp. 307–310.

[71] K. J. Nicholson, W. S. T. Rowe, P. J. Callus, and K. Ghorbani, "Split-ring resonator loading for the slotted waveguide antenna stiffened structure," *IEEE Antennas Wireless Propag. Lett.*, vol. 10, pp. 1524–1527, 2011.

[72] K. J. Nicholson, W. S. T. Rowe, P. J. Callus, and K. Ghorbani, "Split-ring resonator loaded slot array," in *Proc. Asia-Pacific Microw. Conf.*, 2011, pp. 1338–1341.

[73] K. J. Nicholson, W. S. T. Rowe, P. J. Callus, and K. Ghorbani, "Small slot design for slotted waveguide antenna stiffened structure," *Electron. Lett.*, vol. 48, pp. 676–677, 2012.

[74] A. Bojovschi, D. Gray, and K. Ghorbani, "A loop-type end-launcher for carbon fibre reinforced polymer waveguides," *Prog. Electromagn. Res.*, vol. 31, pp. 13–27, May 2013.

[75] A. Bojovschi, A. Galehdar, K. J. Nicholson, P. J. Callus, and K. Ghorbani, "X-band waveguide array fed by a slotted waveguide," in *Proc. Asia–Pacific Microw. Conf.*, 2011, pp. 1206–1209.

[76] K. J. Nicholson, W. S. T. Rowe, P. J. Callus, and K. Ghorbani, "Electronically tunable composite right/left handed transmission line for the Slotted Waveguide Antenna Stiffened Structure," in *Proc. IEEE 7th Int. Congr. Adv. Electromagn. Mater. Microw. Opt.*, 2013, pp. 109–111.

[77] K. Nicholson, W. S. T. Rowe, P. J. Callus, K. Ghorbani, and T. Itoh, "Coaxial right /left-handed transmission line for electronic beam steering in the slotted waveguide antenna stiffened structure," *IEEE Trans. Microw. Theory Techn.*, vol. 62, no. 4, pp. 773–778, Apr. 2014.

[78] K. Nicholson, J. Clough, and K. Ghorbani, "Electronically tunable coaxial right /left handed transmission line for carbon fibre reinforced polymer waveguides," in *Proc. Eur. Microw. Conf.*, 2015, pp. 1104–1107.

[79] K. Ghorbani, T. Baum, K. J. Nicholson, and J. Ahamed, "Advances in aerospace multifunctional structures with integrated antenna structures," in *Proc. Asia-Pacific Microw. Conf.*, 2015, pp. 1–3.

[80] A. Mehdipour, A.-R. Sebak, C. W. Trueman, I. D. Rosca, and S. V. Hoa, "Reinforced continuous carbon-fibre composites using multi-wall carbon nanotubes for wideband antenna applications," *IEEE Trans. Antennas Propag.*, vol. 58, no. 7, pp. 2451–2456, Jul. 2010.

[81] L. Manac'h, X. Castel, and M. Himdi, "Performance of a lozenge monopole antenna made of pure composite laminate," *Prog. Electromagn. Res. Lett.*, vol. 35, pp. 115–123, 2012.

[82] L. Manac'h, X. Castel, and M. Himdi, "Microwave performance of a carbon composite antenna," in *Proc. Eur. Microw. Conf.*, 2013, pp. 770–773.

[83] A. Daliri et al., "A slot spiral in carbon-fibre composite laminate as a conformal load-bearing antenna," *J. Intell. Mater. Syst. Struct.*, vol. 25, pp. 1295–1305, Jun. 2014.

[84] A. Galehdar, P. J. Callus, W. S. T. Rowe, C. H. Wang, S. John, and K. Ghorbani, "Capacitively fed cavity-backed slot antenna in carbon-fiber composite panels," *IEEE Antennas Wireless Propag. Lett.*, vol. 11, pp. 1028–1031, 2012.

[85] A. Mehdipour, T. A. Denidni, A. - R. Sebak, C. W. Trueman, I. D. Rosca, and S. V. Hoa, "Mechanically reconfigurable antennas using an anisotropic carbon-fibre composite ground," *IET Microw., Antennas Propag.*, vol. 7, no. 13, pp. 1055–1063, Oct. 2013.

[86] A. Mehdipour, T. A. Denidni, A. - R. Sebak, and C. W. Trueman, "Reconfigurable TX/RX antenna systems loaded by anisotropic conductive carbon-fiber composite materials," *IEEE Trans. Antennas Propag.*, vol. 62, no. 2, pp. 1002–1006, Feb. 2014.

[87] G. Artner, P. K. Gentner, J. Nicolics, and C. F. Mecklenbräuker, "Carbon fiber reinforced polymer with shredded fibers: Quasiisotropic material properties and antenna performance," *Int. J. Antennas Propag.*, vol. 2017, 2017, Art. no. 6152651.

[88] A. Mark, Y. Xu, and B. T. Dickinson, "Review of microscale flow sensor-enabled mechanosensing in small unmanned aerial vehicles," *J. Aircr.*, vol. 56, no. 3, pp. 962–973, 2019.

[89] S. M. Mangalam, "Phenomena-based real-time aerodynamic measurement system (PRAMS)," in *Proc. IEEE Aerosp. Conf. Proc.*, 2003, pp. 3347–3356.

[90] S. M. Mangalam, "Real-time extraction of hydrodynamic flow characteristics using surface signatures," *IEEE J. Ocean. Eng.*, vol. 29, no. 3, pp. 622–630, Jul. 2004.

[91] H. P. Fei, R. Zhu, Z. Y. Zhou, and J. D. Wang, "Aircraft flight parameters detection based on a neural network using multiple hot-film flow speed sensors," *Smart Mater. Structures*, vol. 16, pp. 1239–1245, 2007.

[92] R. Zhu, P. Liu, X. D. Liu, F. X. Zhang, and Z. Y. Zhou, "A low-cost flexible hot-film sensor system for flow sensing and its application to aircraft," in *Proc. IEEE 22nd Int. Conf. Micro Electro Mech. Syst.*, 2009, pp. 527–530.

[93] P. Liu, R. Zhu, and R. Y. Que, "A flexible flow sensor system and its characteristics for fluid mechanics measurements," *Sensors*, vol. 9, no. 12, pp. 9533–9543, 2009.

[94] R. Que and R. Zhu, "Aircraft aerodynamic parameter detection using micro hot-film flow sensor array and BP neural network identification," *Sensors*, vol. 12, no. 8, pp. 10920–10929, Aug. 2012.

[95] R. Zhu, R. Que, and P. Liu, "Flexible micro flow sensor for micro aerial vehicles," *Front. Mech. Eng.*, vol. 12, no. 4, pp. 539–545, 2017.

[96] M. Zagnoni et al., "A non-invasive capacitive sensor strip for aerodynamic pressure measurement," *Sensors Actuators A, Phys.*, vol. 123, pp. 240–248, 2005.

[97] A. Golfarelli et al., "Acquisition system for pressure sensor network," in *Proc. SENSORS*, 2004, pp. 579–582.

[98] S. Callegari et al., "Aircraft angle of attack and air speed detection by redundant strip pressure sensors," in *Proc. SENSORS*, 2004, pp. 1526–1529.

[99] S. Callegari, M. Zagnoni, A. Golfarelli, and M. Tartagni, "Novel measurement method for air-data system based on strip sensors: Experimental results," in *Proc. SENSORS*, 2005, pp. 1359–1362.

[100] S. Callegari et al., "Experiments on aircraft flight parameter detection by on-skin sensors," *Sensors Actuators A, Phys.*, vol. 130, pp. 155–165, Aug. 2008.

[101] S. Callegari, P. Castaldi, and M. Zanzi, "Parsimonious model for air-data readout from 'On-skin' pressure measurements in subsonic flows," in *Proc. 17th IFAC Symp. Autom. Control Aerosp.*, 2007, pp. 253–258.

[102] N. Gavrilovic, M. Bronz, J. - M. Moschetta, and E. Benard, "Bioinspired wind field estimation–Part 1: Angle of attack measurements through surface pressure distribution," *Int. J. Micro Air Veh.*, vol. 10, 2018, pp. 273–284.

[103] K. T. Wood, S. Araujo-Estrada, T. Richardson, and S. Windsor, "Distributed pressure sensing–based flight control for small fixed-wing unmanned aerial systems," *J. Aircr.*, vol. 56, no. 5, pp. 1951–1960, 2019.

[104] K. T. Borup, T. I. Fossen, and T. A. Johansen, "A machine learning approach for estimating air data parameters for small fixed-wing UAVs using distributed pressure sensors," *IEEE Trans. Aerosp. Electron. Syst.*, vol. 56, no. 3, pp. 2157–2173, Jun. 2020.

[105] A. Mohamed, S. Watkins, R. Clothier, M. Abdulrahim, K. Massey, and R. Sabatini, "Fixed-wing MAV attitude stability in atmospheric turbulence—Part 2: Investigating biologically-inspired sensors," *Prog. Aerosp. Sci.*, vol. 71, pp. 1–13, Nov. 2014.

[106] K. T. Magar et al., "Aerodynamic parameters from distributed heterogeneous CNT hair sensors with a feedforward neural network," *Bioinspiration Biomimetics*, vol. 11, no. 6, 2016, Art. no. 066006.

[107] A. P. J. van Deursen and V. Stelmashuk, "Inductive sensor for lightning current measurement, fitted in aircraft windows—Part I: Analysis for a circular window," *IEEE Sensors J.*, vol. 11, no. 1, pp. 199–204, Jan. 2011.

[108] A. P. J. van Deursen, "Analysis of an inductive sensor for lightning current measurement, fitted in aircraft windows—Part II: Measurements on an A320 aircraft," *IEEE Sensors J.*, vol. 11, no. 1, pp. 205–209, Jan. 2011.

[109] A. P. J. v. Deursen, A. d. Boer, M. Bardet, and J. Boissin, "Window sensor for the A350 and A380 aircraft," in *Proc. Int. Conf. Electromagn. Adv. Appl.*, 2013, pp. 1000–1003.

[110] B. Moslehi, R. J. Black, and F. Faridian, "Multifunctional fibre Bragg grating sensing system for load monitoring of composite wings," in *Proc. Aerosp. Conf.*, 2011, pp. 1–9.

[111] M. Tur et al., "Structural health monitoring of composite-based UAVs using simultaneous fibre optic interrogation by static Rayleigh-based distributed sensing and dynamic fibre Bragg grating point sensors," in *Proc. SPIE*, vol. 9634, 2015, Art. no. 96340P.

[112] C. E. Campanella, A. Cuccovillo, C. Campanella, A. Yurt, and V. M. Passaro, "Fibre Bragg grating based strain sensors: Review of technology and applications," *Sensors*, vol. 18, no. 9, 2018, Art. no. 3115.

[113] E. Abouzeida et al., "Design, manufacture and testing of an FBG-instrumented composite wing," in *Proc. 40th Annu. Rev. Prog. Quantitative Nondestruct. Eval.*, 2014, pp. 1141–1148.

[114] J. M. Costa, "Fibre-optically sensorized composite wing," *Smart Sensor Phenomena, Technol., Netw., Syst. Integration*, vol. 35, 2014, Art. no. 9062.

[115] J. Z. Zhou, Z. H. Cai, L. Kang, B. F. Tang, and W. H. Xu, "Deformation sensing and electrical compensation of smart skin antenna structure with optimal fiber Bragg grating strain sensor placements," *Composite Structures*, vol. 211, pp. 418–432, 2019.

[116] J. Zhou, L. Kang, B. Tang, B. Tang, J. Huang, and C. Wang, "Adaptive compensation of flexible skin antenna with embedded fiber Bragg grating," *IEEE Trans. Antennas Propag.*, vol. 67, no. 7, pp. 4385–4396, Jul. 2019.

[117] R. Matsuzaki, M. Melnykowycz, and A. Todoroki, "Antenna/sensor multifunctional composites for the wireless detection of damage," *Composites Sci. Technol.*, vol. 69, no. 15/16, pp. 2507–2513, Dec. 2009.

[118] Z. Li, A. Haigh, C. Soutis, A. Gibson, and R. Sloan, "Applications of microwave techniques for aerospace composites," in *Proc. IEEE Int. Conf. Microw., Antennas, Commun. Electron. Syst.*, 2017, pp. 1–4.

[119] Z. Li, A. Haigh, C. Soutis, and A. Gibson, "Principles and applications of microwave testing for woven and non-woven carbon fibre-reinforced polymer composites: A topical review," *Appl. Composite Mater.*, vol. 25, no. 4, pp. 965–982, Aug. 2018.

[120] A. Daliri, A. Galehdar, S. John, W. Rowe, and K. Ghorbani, "Circular microstrip patch antenna strain sensor for wireless structural health monitoring," in *Proc. World Congr. Eng.*, 2010, pp. 1173–1178.

[121] A. Daliri, A. Galehdar, W. S. T. Rowe, K. Ghorbani, and S. John, "Utilising microstrip patch antenna strain sensors for structural health monitoring," *J. Intell. Mater. Syst. Structures*, vol. 23, no. 2, pp. 169–182, Jan. 2012.

[122] M. I. R. Shishir, S. Mun, H. - C. Kim, J. W. Kim, and J. Kim, "Frequency selective surface-based chipless passive RFID sensor for detecting damage location," *Struct. Control Health Monit.*, vol. 24, no. 12, Dec. 2017, Art. no. e2028.

[123] A. Alsaadi, J. Meredith, T. Swait, J. L. Curiel-Sosa, Y. Jia, and S. Hayes, "Structural health monitoring for woven fabric CFRP laminates," *Composites B, Eng.*, vol. 174, 2019, Art. no. 107048.

[124] H. S. Shin, L. M. Castano, J. S. Humbert, and S. Bergbreiter, "Sensing skin for detecting wing deformation with embedded soft strain sensors," in *Proc. SENSORS*, 2016, pp. 1–3.

[125] C. K. Kim, L. M. Lee, H. C. Park, W. Hwang, and W. S. Park, "Impact damage and antenna performance of conformal load-bearing antenna structures," *Smart Mater. Structures*, vol. 12, pp. 672–679, 2003.

[126] T. S. Jang, D. S. Oh, J. K. Kim, K. I. Kang, W. H. Cha, and S. W. Rhee, "Electromagnetic performance and impact damage of the microstrip antennas integrated in cylindrical three-dimensional woven composite structures," *Polym. Composites*, vol. 39, no. 9, pp. 3259–3267, Sep. 2018.

[127] H. Kim, M. Park, and K. Hsieh, "Fatigue fracture of embedded copper conductors in multifunctional composite structures," *Composites Sci. Technol.*, vol. 66, no. 7/8, pp. 1010–1021, 2006.

[128] H. Kim and K. Hsieh, "Measurement and prediction of embedded copper foil fatigue crack growth in multifunctional composite structure," *Composites A*, vol. 43, no. 3, pp. 492–506, 2012.

[129] H. Kim and M. Gonzalez, "Fatigue failure of printed circuit board chemically etched copper traces in multifunctional composite structures," *J. Composite Mater.*, vol. 48, no. 8, pp. 985–996, 2014.

[130] J. W. Sabat and A. N. Palazotto, "Structural performance of composite material for a slotted waveguide antenna stiffened structure under compression," *Composite Structures*, vol. 97, pp. 202–210, 2013.

[131] S. M. Baek, M. G. Ko, M. S. Kim, and Y. S. Joo, "Structural design of conformal load-bearing array antenna structure (CLAAS)," *Adv. Composite Mater.*, vol. 26, no. S1, pp. 29–42, Jun. 2017.

[132] S. M. Baek, S. J. Lim, M. G. Ko, M. Y. Park, and M. S. Kim, "Structural design, fabrication and static testing of smart composite skin structure: Conformal load-bearing SATCOM array antenna structure (CLSAAS)," *Int. J. Aeronaut. Space Sci.*, vol. 21, pp. 50–62, 2020.

[133] R. Kothari and C. T. Sun, "Design and analysis of multifunctional structures with embedded electronics for thermomechanical loads," *J. Sandwich Structures Mater.*, vol. 14, pp. 734–752, 2012.

[134] K. Sairajan, G. Aglietti, and K. Mani, "A review of multifunctional structure technology for aerospace applications," *Acta Astronautica*, vol. 120, pp. 30–42, 2016.

[135] S. P. Rawal, D. M. Barnett, and D. E. Martin, "Thermal management for multifunctional structures," *IEEE Trans. Adv. Packag.*, vol. 22, no. 3, pp. 379–383, Aug. 1999.

[136] T. S. Jang, D. S. Oh, J. K. Kim, K. I. Kang, W. H. Cha, and S. W. Rhee, "Development of multi-functional composite structures with embedded electronics for space application," *Acta Astronaut.*, vol. 68, pp. 240–252, 2011.

[137] J. Zhou, J. Huang, Q. He, B. Tang, and L. Song, "Development and coupling analysis of active skin antenna," *Smart Mater. Structures*, vol. 26, no. 2, 2016, Art. no. 025011.

[138] C. E. Jones et al., "Electrical and thermal effects of fault currents in aircraft electrical power systems with composite aero-structures," *IEEE Trans. Transport. Electrific.*, vol. 4, no. 3, pp. 660–670, Sep. 2018.

[139] R. Malmqvist, A. Ouacha, and R. Erickson, "Multi-band and reconfigurable front-ends for flexible and multi-functional RF systems," in *Proc. Asia–Pacific Microw. Conf.*, 2007, pp. 1–4.

[140] M. Garcia et al., "Modeling and simulation of a photovoltaic array for a fixed-wing unmanned aerial vehicle," in *Proc. IEEE 43rd Photovoltaic Specialists Conf.*, 2016, pp. 2682–2687.

[141] I. Ridwan, "The effect of use of solar panels on micro scale fixed - wing UAV type as a power recharging system," in *Proc. 3rd Int. Conf. Nucl. Energy Techn. Sci.*, 2019, Art. no. 020044.

[142] F. Zhang, R. Zhu, P. Liu, W. Xiong, X. Liu, and Z. Zhou, "A novel Micro Air Vehicle with flexible wing integrated with on-board electronic devices," in *Proc. IEEE Conf. Robot., Automat. Mechatron.*, 2008, pp. 252–257.

[143] P. Pa, M. S. Mirotznik, and S. Yarlaggada, "High frequency characterization of conductive inks embedded within a structural composite," in *Proc. IEEE Int. Symp. Antennas Propag. USNC/URSI Nat. Radio Sci. Meeting*, 2015, pp. 1310–1311.

[144] G. Beziuk, T. C. Baum, K. Ghorbani, and K. J. Nicholson, "RF signal multiplexer embedded into multifunctional composite structure," *IEEE Trans. Microw. Theory Techn.*, vol. 67, no. 12, pp. 4935–4943, Dec. 2019.

[145] T. C. Baum, K. Ghorbani, R. W. Ziolkowski, and K. J. Nicholson, "Investigation of microwave active elements embedded in composite structures," in *Proc. IEEE MTT-S Int. Microw. Symp.*, 2016, pp. 1–3.

[146] T. C. Baum, R. W. Ziolkowski, K. Ghorbani, and K. J. Nicholson, "Embroidered active microwave composite preimpregnated electronics—Pregtronics," *IEEE Trans. Microw. Theory Techn.*, vol. 64, no. 10, pp. 3175–3186, Oct. 2016.

[147] T. C. Baum, R. W. Ziolkowski, K. Ghorbani, and K. J. Nicholson, "Investigation of a conformal amplifier embedded in an aerospace composite structure," in *Proc. 47th Eur. Microw. Conf.*, 2017, pp. 588–591.

[148] G. Beziuk, T. C. Baum, K. Ghorbani, and K. J. Nicholson, "Multifunctional composite RF four-way switch," in *Proc. IEEE MTT-S Int. Microw. Symp.*, 2019, pp. 1088–1091.

[149] K. Nicholson, O. Dunbabin, T. Baum, and K. Ghorbani, "Characterisation of integrated microstrip lines in aerospace composite structure," *Electron. Lett.*, vol. 53, no. 1, pp. 36–38, Jan. 2017.

[150] R. L. Chaney and D. R. Hackler, Advanced conformal load-bearing antenna structures, American Semiconductor, Inc,Boise, ID, USA, 2012.

[151] H. S. Kim, S. Jin, J. S. Park, H. T. Hahn, H. C. Jung, and J. W. Joung, "Inkjet printed electronics for multifunctional composite structure," *Composites Sci. Technol.*, vol. 69, pp. 1256–1264, 2009.

[152] J. Ahamed, C. Wang, S. John, and P. Callus, "A novel concept for conformal load-bearing antenna structures using dissimilar composites," in *Proc. Int. Conf. Composite Mater.*, 2013, pp. 7494–7495.

[153] J. Ahamed, M. Joosten, and C. Wang, "Novel hybrid co-cured carbon/glass fibre composite joints for safety critical structures," in *Proc. Int. Conf. Composite Mater.*, 2015, pp. 1–12.

[154] J. Ahamed, M. Joosten, P. Callus, S. John, and C. H. Wang, "Ply-interleaving technique for joining hybrid carbon/glass fibre composite materials," *Composites A, Appl. Sci. Manuf.*, vol. 84, pp. 134–146, 2016.

[155] J. Ahamed, M. Joosten, P. Callus, M. R. Winsom, and C. H. Wang, "Ply-overlap hybrid technique for joining dissimilar composite materials," *Mater. Des.*, vol. 100, pp. 157–167, 2016.

[156] J. Ahamed, 1st Jul 2018. Disses, RMIT Univ., Melbourne, VIC, Australia, 2018.

[157] K. Nicholson, T. C. Baum, and K. Ghorbani, "Conformal voronoi metasurface antenna embedded in a composite structural laminate," *IEEE Trans. Antennas Propag.*, vol. 69, no. 7, pp. 3717–3725, Jul. 2021.

[158] Z. Li, K. Wang, Y. Lv, S. Qian, X. Zhang, and X. Cui, "Wing conformal load-bearing endfire phased array antenna skin technology," *IEEE Trans. Antennas Propag.*, vol. 71, no. 3, pp. 2064–2069, Mar. 2023.

[159] X. Wei et al., "Carbon fibre composite honeycomb structures and the application for satellite antenna reflector with high precision advances in astronautics," *Adv. Astronaut. Sci. Technol.*, vol. 5, pp. 423–441, 2022.

[160] A. Patil and E. J. Arnold, "Characterization of standard structural CRFP beam shapes for UAS VHF antenna applications," *AIAA SciTech Forum*, Jan. 2021, doi: 10.2514/6.2021-1803.vid.

[161] A. Patil and E. J. Arnold, "Characterizing carbon fiber conductivity for structural antenna applications," *IEEE Trans. Antennas Propag.*, vol. 70, no. 1, pp. 451–458, Jan. 2022.

[162] P. Ravindra, B. N. Ravishankar, S. Dasgupta, and K. Selvanayaki, "Conformal reflector backed printed dipole antenna for directional UAV communications," in *Proc. IEEE 4th Int. Conf. Commun. Electron. Syst.*, 2019, pp. 1613–1617.

[163] W. Zhao, Y. Xie, Q. Yan, Z. Xie, and P. Zhangc, "Damage tolerance-based design of conformal antenna composite structure," *Mechanics Adv. Mater. Structures*, vol. 29, no. 26, pp. 5530–5541, 2022.

[164] V. Platero, "2-in-1 smart panels: Multifunctional structures with embedded patch antennas," *Acta Astronautica*, vol. 175, pp. 51–56, 2022.

[165] E. Arnold, A. Patil, F. Rodriguez-Morales, and V. Occhiogrosso, "Near-high frequency antenna for unmanned aerial system ice-penetrating radar," *Microw. Opt. Technol. Lett.*, vol. 64, pp. 1077–1083, 2022.

[166] J. W. Burns, E. J. Arnold, and U. Ballingu, "Weight-optimized structural antenna concept for UAS remote sensing," *AIAA SCITECH 2022 Forum*, 2022, doi: 10.2514/6.2022-2556.vid.

[167] Z. Liu, S. Wang, J. Shao, W. Zhao, G. Yu, and L. Wum, "3D radar stealth composite hierarchical grid structure with extremely broadband absorption performance and effective load bearing," *Composites B*, vol. 247, 2022, Art. no. 110316.

[168] K. J. Nicholson, O. Dunbabin, T. Baum, and K. Ghorbani, "Characterisation of integrated microstrip lines in aerospace composite structure," *Electron. Lett.*, vol. 53, no. 1, pp. 36–33, Jan. 2017.

[169] J. N. Borges, "Functionalization of copper surfaces by plasma treatments to improve adhesion of epoxy resins," *Plasma Process. Polym.*, vol. 6, pp. S490–S495, 2009.

[170] X. Guo, S. Lin, and F. Dai, "A metal hybrid bistable composite tube for multifunctional and reconfigurable antenna," *Composites Sci. Technol.*, vol. 233, 2023, Art. no. 109887.

[171] D. Chopda, "Design and development of S band radio frequency (RF) cavity filter using carbon fibre reinforcement polymer (CFRP) material for communication satellites," in *Recent Advances in Manufacturing Processes and Systems*, H. K. Dave Ed. Singapore: Springer, 2022, pp. 253–263.

[172] J. Brooks, "Multiobjective optimization and analysis of slotted waveguide antenna stiffened structures," Ph.D. dissertation, Virginia Polytechnic Inst. State Univ.,Blacksburg, VA, USA, Sep. 2022.

[173] R. Healey, K. J. Nicholson, J. Wang, J. Patniotis, T. Lynch, and W. K. Chiu, "Conformal load-bearing antenna structures - Mechanical loading considerations," *Sensors*, vol. 22, no. 1, Jan. 2022, Art. no. 48.

[174] A. J. Good, D. Roper, B. Good, S. Yarlagadda, and M. S. Mirotznik, "Multifunctional graded dielectrics fabricated using dry powder printing," *Smart Mater. Structures.*, vol. 26, no. 9, Sep. 2017, Art. no. 095036.
[175] C. Miron, P. Mele, S. Kaneko, and T. Endo, *Carbon-Related Materials*. New York, NY, USA: Springer, 2020.
[176] X. Z. Gao, Z. X. Hou, Z. Guo, and X. Q. Chen, "Reviews of methods to extract and store energy for solar-powered aircraft," *Renewable Sustain. Energy Rev.*, vol. 44, pp. 96–108, 2015.
[177] X. Zhu, Z. Guo, and Z. Hou, "Solar-powered airplanes: A historical perspective and future challenges," *Prog. Aerosp. Sci.*, vol. 71, pp. 36–53, 2014.
[178] N. R. Khan, A. V. Raghorte, P. V. Nandankar, and J. A. Waware, "Solar powered UAV: A comprehensive review," in *AIP Conf. Proc.*, vol. 2753, 2023, Art. no. 020016.
[179] G. Beziuk, T. C. Baum, K. Ghorbani, and K. N. Nicholson, "Structurally Integrated radar in an aerospace composite laminate," *IEEE Trans. Compon., Packag. Manuf. Technol.*, vol. 11, no. 11, pp. 1835–1843, Nov. 2021.

GRZEGORZ BEZIUK (Member, IEEE) was born in Wrocław, Poland, in 1974. He received the M.Sc.Eng. and Ph.D. degrees in electronics and telecommunication from Wrocław University of Science and Technology, Wrocław, Poland, in 1999 and 2005, respectively. From 1999 to 2013, he was a Research Assistant, Lecturer, and then an Assistant Professor with the Faculty of Electronics, Wrocław University of Technology. In 2014, he joined the Mass Spectrometry Laboratory, Department of Physics, The University of Auckland, Auckland, New Zealand, as a Research Engineer. From 2015 to 2018, he was a Process and Test Engineer with the TriCab Pty. Ltd. Group, Melbourne, VIC, Australia, where he was working on the improvement of the production process of power and instrumentation cables and cable accessories. In 2018, he joined the Royal Melbourne Institute of Technology, Melbourne, as a Research Officer. Since 2022, he has been with the Australian Department of Defence, Defence Science and Technology Group, Port Melbourne, VIC, Australia. He successfully collaborated with many industrial partners and scientific institution, notably CERN, Geneva, Switzerland and GSI, Darmstadt, Germany, where he was working on fault diagnostics of superconducting and normal conducting magnets of LHC and FAIR particle accelerators. His research interests include electronic circuits, microwaves and THz techniques, RF circuit fabrication methods, instrumentation and measurement techniques, and electromagnetic geophysical methods.

ANDREW KRAJEWSKI (Member IEEE) received the master's degree in electronics from the University of Science and Technology, Krakow, Poland, in 1978, and the Doctorate degree from Deakin University, Melbourne, VIC, Australia, in 2007, in the area of automation of industries. Since then, he has carried out multiple duties at the level of the Senior Research Scientist with the areas of applied electronic, software development, RF shielding, carbon fibers and composite structures with, national/international partners, including Australian Defence Departments. Since 2011, he has been the Project Leader by the Commonwealth Scientific Industry and Research Organization with regards to an industry automation related project. Since 2019, he has been with the Royal Melbourne Institute of Technology, Melbourne, VIC, Australia, where he held variety research positions. During this time, he contributed to the development of the Cl2 (chlorine gas) sensing system for Australian Defence Force and was involved in various simulations/designs of the Multifunctional Arrays RF project funded by the Australian Defence Science and Technology department. His research interests include conformal RF components, wearable RF components, RF shielding, harmful volatile substances detection, antenna arrays control systems, and carbon composites.

THOMAS C. BAUM (Member IEEE) received the B.Eng. degree in aerospace engineering (Hons.) and the Ph.D. degree in electrical engineering from RMIT University, Melbourne, VIC, Australia, in 2009 and 2014, respectively, in the field of EM microwave materials and scattering. In 2015, he became a Research Fellow with RMIT University, working on a variety of microwave related research areas including conformal load bearing antenna structures [funded by DSTO, now Defence Science and Technology (DST)], coherent Doppler tomography, low cost radar systems, and dielectric material characterization. In 2017, he joined the Multifunctional Materials Group, Platforms Division of DST Group. Since 2014, he has been an active member of the organizing committee for the Australian Microwave Symposium, Asia Pacific Microwave Conference, and Radio Frequency Integrated Technologies, when held in Australia. His research interests include novel antenna designs, radar systems, radar absorbing applications, scattering phenomena, microwave measurement techniques, material characterization, additive manufacturing and novel applications of these areas for multifunctional composite structures.

KELVIN J. NICHOLSON (Senior Member IEEE) received the B.Sc. degree in physics and the B.Eng. (Hons.) degree in electrical engineering from the University of Melbourne, Melbourne, VIC, Australia, in 2005, and the Ph.D. degree in electrical engineering from RMIT University, Melbourne, with the support of the Defence Science and Technology (DST) Enabling Research Program in 2014. In 2006, he joined the Australian Department of Defence - DST as part of the Aerospace Composite Technologies Group, Aerospace Division. He has led the development of new microwave Doppler tomography imaging techniques for the assessment of damaged and repaired composite structures. His research interests include DST include advanced composite materials and manufacturing techniques for electromagnetic applications. He has assisted with the mitigation of electromagnetic interference issues aboard the ANZAC frigates and was awarded a Chief Defence Scientist Commendation in 2011 and a Royal Australian Navy Commendation in 2012. Dr. Nicholson was awarded a Defence International Fellowship in 2019 to pursue a twelve month posting at The University of Delaware Newark, DE, USA, where he developed new methods to manufacture conformal metasurface antennas.

KAMRAN GHORBANI (Senior Member IEEE) received the B.Eng. (Hons.) and Ph.D. degrees from RMIT University, Melbourne, VIC, Australia, in 1994 and 2001, respectively. From November 1994 to 1996, he was a graduate RF Engineer with AWA Defence Industries, working on early warning radar systems. In 1996, he joined RMIT University to pursue his Ph.D. studies. From 1999 to 2001, he was a Senior RF Engineer with Tele-IP, working on VHF transceivers for commercial aircraft. In 2001, he joined the Department of Communication and Electronic Engineering (now the School of Engineering), RMIT University as a continuing Academic.

He is the Research Leader of the RF & Antennas Research Group, RMIT University. He is responsible for strategic planning and managing the research group. His research interests include multifunctional microwave structures, microwave sensors, frequency selective surfaces, metamaterials, RF energy harvesting, and radar systems.

Dr. Ghorbani was the Chair of the Asia Pacific Microwave Conference APMC2011, which was held in Melbourne. He was the Co-Chair of the Technical Program Committee for the IEEE International Microwave and RF Conference, IMaRC2014, which was held in India. He was the Chair of the first Australian Microwave Symposium, AMS2014, which was held in Melbourne, Australia. He was the Chair of the Technical Program Committee of the Asia Pacific Microwave Conference APMC2016, which was held in India. He was an Associate Editor for IEEE TRANSACTIONS ON MICROWAVE THEORY AND TECHNIQUES and *IET Microwaves, Antennas & Propagation*.